ARTICLE

Check for updates

A succession of near-orthogonal horizontal tectonic shortenings in the Paleoproterozoic Central Lapland Greenstone Belt of Fennoscandia: constraints from the world-class Suurikuusikko gold deposit

M. Sayab[1] · F. Molnár[1] · D. Aerden[2] · T. Niiranen[3] · J. Kuva[1] · J. Välimaa[4]

Abstract

The relative and absolute timing of orogenic gold deposits in complex structural settings are active and challenging topics of research, especially in Precambrian greenstone belts. The Suurikuusikko gold deposit in Central Lapland Greenstone Belt is currently the largest primary gold producing deposit in Europe, located on a slight bend of the strike-slip Kiistala shear zone (KiSZ). Gold is refractory and locked inside arsenopyrite and pyrite. In this study, different structural features were investigated along the KiSZ from the recently stripped Etelä pit, which is the southern extension of the Suurikuusikko ore body. Our data source ranges from aeromagnetic to high-resolution aerial images, X-ray computed tomography scans of selected rock samples and regional geological and geophysical datasets. The KiSZ has recorded five discrete deformation phases, spanning between ca. 1.92 and 1.76 Ga. The refractory gold at the Suurikuusikko deposit formed during E-W contraction related to the D1 thrusting phase. This was followed by a N-S shortening event (D2), where most of the strain was taken up by the northern and southern thrusts. Tectonic vectors then switched from N-S to NE-SW and, as a result, dextral strike-slip regime (D3) commenced along the KiSZ. This event exsolved invisible gold from the sulfides and remobilized it along with fractures. A near-orthogonal switch of the regional stress regime from NE-SW to NW-SE flipped the kinematics of the KiSZ from dextral to sinistral (D4). The last deformation phase (D5) produced widespread veining under E-W contraction and secured gold mineralization at the Iso-Kuotko gold deposit within the KiSZ.

Keywords Orogenic gold · Tectonics · UAV · X-ray tomography · Greenstone belt

✉ M. Sayab
   sayab.muhammad@gtk.fi

1   Geological Survey of Finland, P.O. Box 96, FI-02151 Espoo, Finland

2   Departamento de Geodinámica and IACT-CSIC, Universidad de Granada, 18002 Granada, Spain

3   Geological Survey of Finland, P.O. Box 77, FI-96101 Rovaniemi, Finland

4   Agnico Eagle, Kittilä Mine, FI-99250 Kiistala, Finland

Introduction

Research during the past two decades has shown that the localization of world-class orogenic gold deposits in metamorphic belts are intimately related to the repetitive reworking of crustal-scale compressional shears (e.g., Groves et al. 1998, 2018; Goldfarb et al. 2005; Tomkins 2013; Groves and Santosh 2016; Sayab et al. 2016). However, determining the relative and absolute timing of gold mineralization and fluid flow with respect to the kinematic evolution of these shear zones can be challenging (e.g., Blewett et al. 2010; Vielreicher et al. 2016), especially in regions of long-lived orogenesis (e.g. Sayab 2008; Molnár et al. 2018). This is partly because of multiple reactivations of these shear zones and associated fluid flow, heterogeneous at different scales due to the partitioning of deformation (Bell 1986; Aerden 1993;

Deng et al. 2016). In such shear zone systems, the remobilization and deposition of ore minerals by ore-carrying fluids are controlled by both proximal and far-field stresses (e.g., Blenkinsop and Doyle 2014; Blenkinsop et al. 2017) and axiomatically linked metamorphic conditions (Yardley and Cleverley 2015).

Present-day exposure levels of Archean and Paleoproterozoic terranes commonly offer outcrops that preserve windows into deep levels of ancient crust for investigating the interplay between the structural history and relative timing of gold mineralization. In this study, we have attempted to resolve the kinematic evolution of the world-class Suurikuusikko gold deposit, which is located within the Paleoproterozoic Central Lapland Greenstone Belt (CLGB) of northern Finland (Fig. 1a). The deposit lies in the middle of the roughly 25-km long Kiistala shear zone (KiSZ), which is generally characterized as a strike-slip fault (Patison et al. 2007). The high-resolution aeromagnetic map (Fig. 1b) shows that the deposit is located at a slight bend in this shear zone. The Kittilä mine on the Suurikuusikko gold deposit is currently the largest primary gold producing mine in Europe; it is proven and probable mineral reserves being 4.1 million ounces of gold (27 Mt @ 4.74 g/t Au) as of December 31, 2017, with an estimated mine life till 2035: https://www.agnicoeagle.com/English/home/default.aspx. The Iso-Kuotko deposit, located approximately 12 km to the north of Suurikuusikko along the KiSZ, shows significantly different mineralogy and style of gold mineralization (Molnár et al. 2018).

Given the scarcity of outcrops in the CLGB due to dense vegetation and sedimentary cover, our structural analysis focuses on the recently stripped Etelä open pit, which is located about ~ 2 km south of the main Suurikuusikko ore body along
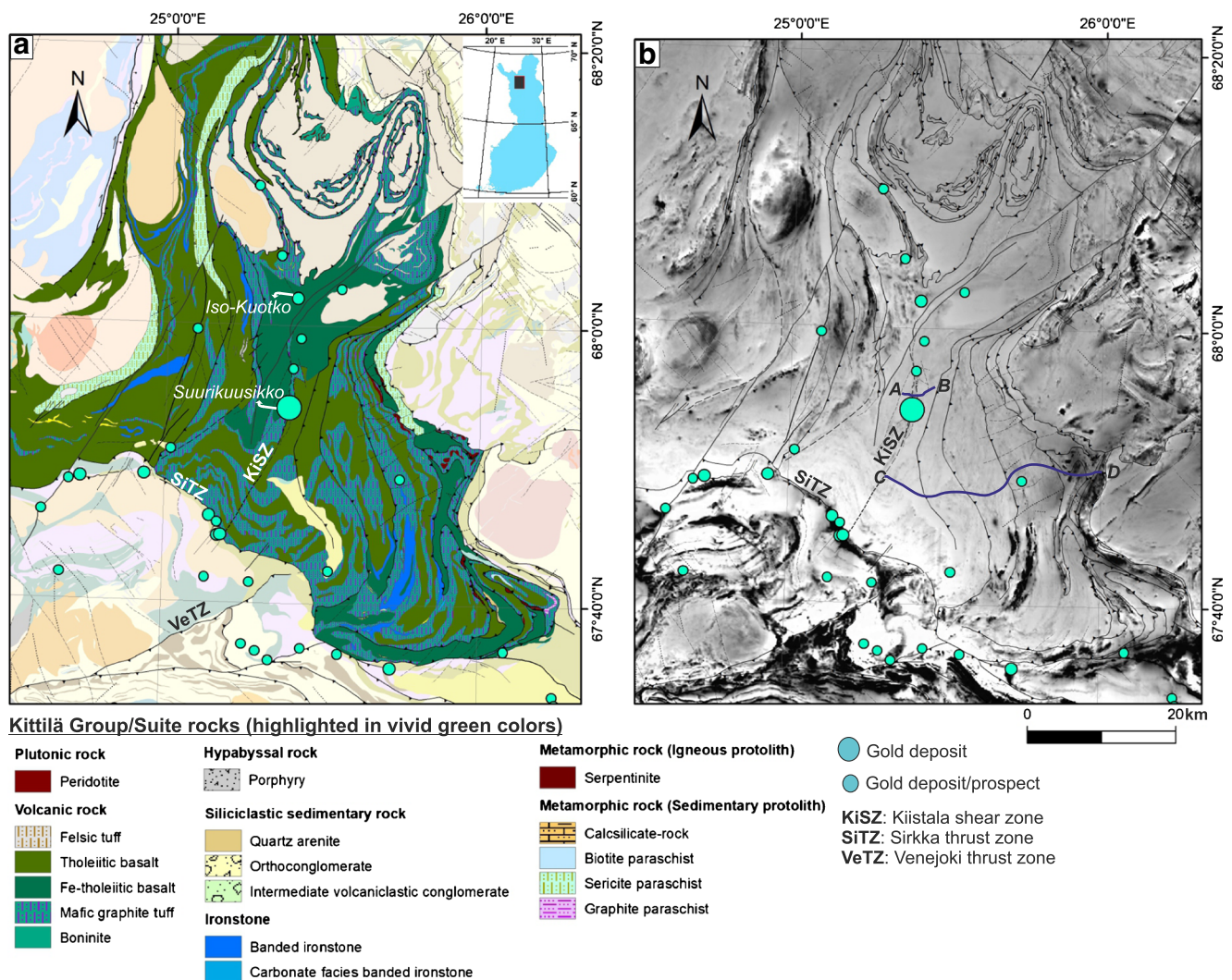

Kittilä Group/Suite rocks (highlighted in vivid green colors)

Plutonic rock
- Peridotite

Volcanic rock
- Felsic tuff
- Tholeiitic basalt
- Fe-tholeiitic basalt
- Mafic graphite tuff
- Boninite

Hypabyssal rock
- Porphyry

Siliciclastic sedimentary rock
- Quartz arenite
- Orthoconglomerate
- Intermediate volcaniclastic conglomerate

Ironstone
- Banded ironstone
- Carbonate facies banded ironstone

Metamorphic rock (Igneous protolith)
- Serpentinite

Metamorphic rock (Sedimentary protolith)
- Calcsilicate-rock
- Biotite paraschist
- Sericite paraschist
- Graphite paraschist

○ Gold deposit
○ Gold deposit/prospect

KiSZ: Kiistala shear zone
SiTZ: Sirkka thrust zone
VeTZ: Venejoki thrust zone

Fig. 1 **a** Geological and structural map of the Central Lapland Greenstone Belt (CLGB) showing locations of major orogenic gold deposits and prospects (circles). The Kittilä group rocks are highlighted in green, in different shades, in the middle of the map (simplified from the Geological Survey of Finland Digital bedrock database). **b** Aeromagnetic map of the same area shown in panel **a**. The Kittilä Group is bounded by tectonic boundaries. Suurikuusikko (A–B) and Petäjäselkä (C–D) reflection seismic lines are shown on the map. KiSZ, Kiistala shear zone; SiSZ, Sirkka thrust zone; VeTZ, Venejoki thrust zone

the same shear zone. The Etelä pit provides the second largest bedrock exposure in the CLGB after the Suurikuusikko open pit, but the latter was not accessible for our research due to mining activities. Although, our main focus is on the Etelä pit, we also discuss the timing of gold mineralization at the Iso-Kuotko deposit (Molnár et al. 2018).

Besides conventional field observations and geological mapping, we imaged the whole Etelä pit using an unmanned aerial vehicle (UAV) flying at low altitude to generate a three-dimensional model (3D) of the pit. The purpose was to present an aerial image of the shear zone at an ultra-high resolution (8.8 mm/pixel). For multi-scale structural analysis, the aerial and field observations were coupled to X-ray computed tomography scans of selected rock samples and high-fidelity reflection seismic profiles across the KiSZ. In addition, the availability of fine-resolution aeromagnetic images of the CLGB along with published regional geology (Nironen 2017) and the known tectonic setting of the area (Sayab et al. 2017; Lahtinen et al. 2018) has allowed us to extend our open-pit data and interpretations to the regional scale. Consequently, we present a first synoptic tectonic model for the KiSZ with emphasis on the Suurikuusikko gold deposit within the framework of the CLGB and the Svecofennian orogeny (ca. 1.92–1.76 Ga). The model strengthens our understanding of the formation of orogenic gold deposits in greenstone belts in general. As highlighted above, we have used a variety of tools at different scales to reconstruct the kinematic evolution of the KiSZ.

Geological setting

The volcano-sedimentary succession of the Paleoproterozoic CLGB of northern Finland is divided into five lithostratigraphic groups (Lehtonen et al. 1998) between ca. 2.4 and 2.0 Ga (Hanski and Huhma 2005). These are, from oldest to youngest, the Salla, Onkamo, Sodankylä, Savukoski, and Kittilä groups. Additionally, the Lainio and Kumpu groups have been attributed to a molasse-like sedimentary package deposited after ca. 1880 Ma (Hanski and Huhma 2005). The CLGB hosts at least 30 gold occurrences (Eilu 2007) mostly along with two perpendicularly intersecting prominent shear zones, namely the NNE-SSW-trending KiSZ and WNW-ESE-striking Sirkka thrust zone or "Sirkka Line" (Gaál et al. 1989; Luosto et al. 1989) (Fig. 1). The latter is defined by a S- to SW-dipping (~40°) imbricate thrust stack that separates the Savukoski and Kittilä groups (Fig. 1a) (Lehtonen et al. 1998).

The Suurikuusikko gold deposit is hosted by ca 2.0 Ga Kittilä group rocks (or Kittilä Suite) (Luukas et al. 2017), which is estimated to reach a thickness of up to 9 km as measured from geological, geophysical, and seismic data (Niiranen 2015). The supracrustal rocks in the Kittilä Group have been divided into four formations (Lehtonen et al. 1998), from bottom to top, the Kautoselkä formation, Porkonen

formation, Vesmajärvi formation, and Pyhäjärvi formation. The Kautoselkä formation is mainly composed of tholeiitic basalts with minor proportions of metagreywackes, phyllites, graphite- and sulfide-bearing schists, and carbonate rocks. The volcanic rocks of the Vesmajärvi formations are komatiitic basalts and basaltic andesites. Geochemical relationships suggest that the metavolcanic rocks of the Kautoselkä and Vesmajärvi formations do not share a common magma source (Lehtonen et al. 1998; Hanski and Huhma 2005). The Porkonen formation consists of banded iron formation, iron-sulfide, and iron-carbonate schist, whereas the Pyhäjärvi formation consists of mica schist and greywacke. The Kittilä group is thought to be derived from a complex of island arcs and oceanic plateaus accreted to a continental margin (Hanski and Huhma 2005). The metamorphic grade of the Kittilä group is greenschist facies, accompanied by carbonate, chlorite, sericite, and albite alteration, especially along the Kiistala and Sirkka shear zones (Hölttä et al. 2007).

Ages of gold mineralization and hydrothermal events at the Suurikuusikko and Iso-Kuotko deposits fall into three broad groups: ca. 1.92–1.91 Ga, 1.87–1.86 Ga, and 1.77–1.76 Ga (Rastas et al. 2001; Molnár et al. 2018). Most of the gold at Suurikuusikko is refractory and resides in arsenopyrite (73.2%) and pyrite (22.7%), whereas 4.1% occurs as free gold (Kojonen and Johanson 1999). A 3D investigation using synchrotron X-ray nanotomography of the arsenopyrite crystals from Suurikuusikko indicated that inclusions of native gold grains are associated with rutile or localized along fractures inside arsenopyrite crystals (Sayab et al. 2016), but coupled As-Sb-Au concentrations determined by LA-ICP-MS analyses indicate that majority of gold is accommodated by the crystal structure of arsenopyrite and pyrite (Molnár et al. 2018). Koppström (2012) and Wyche et al. (2015) characterized four generations of arsenopyrite and pyrite based on textural and compositional variations and noted that gold is mainly associated with the second stage of sulfidation. In contrast, only about 20% of gold ore is refractory at Iso-Kuotko and most of the visible gold is confined to late brittle fractures (Härkönen et al. 2000).

Structural overview

The first schematic tectonic model for the CLGB was presented by Ward et al. (1989), who suggested a foreland fold and thrust belt-type setting related to the Svecofennian orogeny (ca. 1.92–1.77 Ga). According to their model, the greenstone belt was sandwiched between the granulite belt of Lapland in the NE and the Central Lapland Granitoid Complex (CLGC) in the S-SW, whereas N-NE trending dextral shear zones in the CLGB are reactivated pre-existing transfer faults.

Lehtonen et al. (1998) recognized the earliest Proterozoic deformation in the form of metamorphic mineral growth accompanied by incipient folding and thrusting. They suggested that this was the "main deformation stage," that it was

characterized by tight folds and that its maximum age was ca. 1.89 Ga. In their deformation scheme, a third phase generated N-S trending folds with vertical axial planes as a result of E-W horizontal contraction. This is followed by the exhumation and deposition of molasse-type Kumpu group sediments. A fourth deformation episode formed E-W trending folds in the region involving Kumpu group sediments without a notable metamorphic overprint.

Väisänen (2002) and Hölttä et al. (2007) recognized three deformation events (D1–D3) in Central Lapland. In their scheme, the earliest fabric (S1) corresponds to a bedding-parallel foliation preserved within F2 fold hinges and as inclusion trails within porphyroblasts. S2, the main foliation in the region, is axial planar to tight to isoclinal recumbent folds. S2 is shallowly dipping and is characterized by chlorite and muscovite in low-grade rocks and biotite in higher-grade rocks. Based on F2 fold vergence, they interpreted northward transport direction along the Sirkka thrust zone (Fig. 1) at ca. 1.88–1.87 Ga. Their D3 event explains folds with a heterogeneous distribution in the study region and variable E-W, N-S, NE-SW, and NNW-SSE striking axial planes with E-W and N-S being the dominant directions (Fig. 1). They further classified the region into six metamorphic zones from greenschist facies in the core of the CLGB to the surrounding amphibolite and granulite facies zones.

Patison (2007) and Patison et al. (2007) attributed the D1 and D2 events of Hölttä et al. (2007) to the same thrusting event. Their D3 is associated with strike-slip shear zones, including the KiSZ. D4 corresponds to late-orogenic faults that cut the post-collisional Nattanen-type granites of ca. 1.77 Ga. The kinematics of the KiSZ remains uncertain, though. Patison et al. (2007) inferred early sinistral shearing followed by later dextral overprint based on aeromagnetic data. Ward et al. (1989) proposed only dextral strike-slip shearing along N-NE trending shear zones in the CLGB. Based on drill core gold assay data, a positive correlation has been found between the strike-slip KiSZ and the concentration of gold present in host rocks at the Suurikuusikko gold deposit (Patison et al. 2007).

An overarching tectonic scenario for the evolution of the CLGB (Fig. 1) was recently presented by Nironen (2017), which is similar to the tectonic model of Lahtinen et al. (2015), and includes the six ductile deformation events in the Kittilä Suite rocks. (1) Initial (ca. 1.93–1.92 Ga) collision between the Norrbotten and Karelia lithospheric blocks, wherein thrusting from the west yielded a fold and thrust belt involving the Kittilä Suite and adjacent domains. (2) Continued E-W shortening generated large-scale folding with N-S striking axial planes. (3) A near-orthogonal switch in the tectonic shortening from E-W to N-S due to a collision between the Lapland-Kola and Karelia lithospheric blocks further sandwiching the Kittilä Suite rocks. The relative timing of the second and third deformation events was unresolved both falling within the time

frame of ca. 1.92 to 1.89 Ga. (4) D4 structures were generated following an acute shift in the direction of tectonic shortening from N-S (event 3) to NE-SW and south at ca. 1.88–1.87 Ga. (5) The last ductile deformation involved NW-SE contraction (ca. 1.84–1.83 Ga) that caused folding in the region, and was followed by (6) orogenic collapse from ca. 1.80 to 1.77 Ga.

Similarly, five regional deformation events in the timeframe of ca. 1.92–1.76 Ga were proposed by Lahtinen et al. (2018) in the Paleoproterozoic Central Lapland Granitoid Complex, which is situated south of the CLGB. Overall, the tectonic shortening vectors are the same as proposed by Nironen (2017) for the CLGB with only slight age differences. However, the D5 event of Lahtinen et al. (2018) in the Central Lapland Granitoid Complex occurred after the orogenic collapse stage (ca. 1.80–1.77 Ga).

Study methods

Unmanned aerial vehicle (UAV) data acquisition and field observations

UAV-based, close-range digital photogrammetry is becoming an increasingly popular technique in the structural mapping of exposed rock surfaces and open-pit mines (e.g., Sayab et al. 2018). In this study, we have followed the well-established protocols of "Structure-from-Motion" with "Multi-View Stereopsis" (SfM-MVS) workflow to generate a high-spatial-resolution 3D model of the Etelä pit (Snavely et al. 2008; Westoby et al. 2012; Bemis et al. 2014; Sayab et al. 2018). We used DJI's Phantom 4 Professional (P4P) quadcopter to capture high-spatial-resolution overlapping aerial images to cover the areal extent of the pit (Fig. 2). The P4P is equipped with an electronically stabilized 12-megapixel resolution digital camera. Two hundred fifty-one aerial images were acquired at an altitude of about 24 m from the ground surface. The camera stations were kept orthogonal to the surface with an effective overlap of > 80% (Fig. 2a). An area of about 0.0155 km^2 was covered in about 45 min.

All the images were processed in Agisoft PhotoScan Professional 1.2.4 (hereafter referred to as PhotoScan). PhotoScan is based on SfM-MVS algorithm, which automatically detects a suite of tie points in overlapping multiple image pairs to generate a dense 3D point cloud (http://www.agisoft.com/). Eight ground control points (GCPs) were placed around the pit for georeferencing and scaling purposes and measured using a high-precision RTK GPS (Leica Viva GS14 geosystem, https://leica-geosystems.com/fi-FI/) before the aerial survey (Fig. 2b–d). All 251 images were imported into PhotoScan and inspected through the quality check function to detect and remove blurry images. None of the images failed the quality test and were used in the subsequent image alignment and dense point cloud modeling processing steps. Photoscan yielded 14,650,432
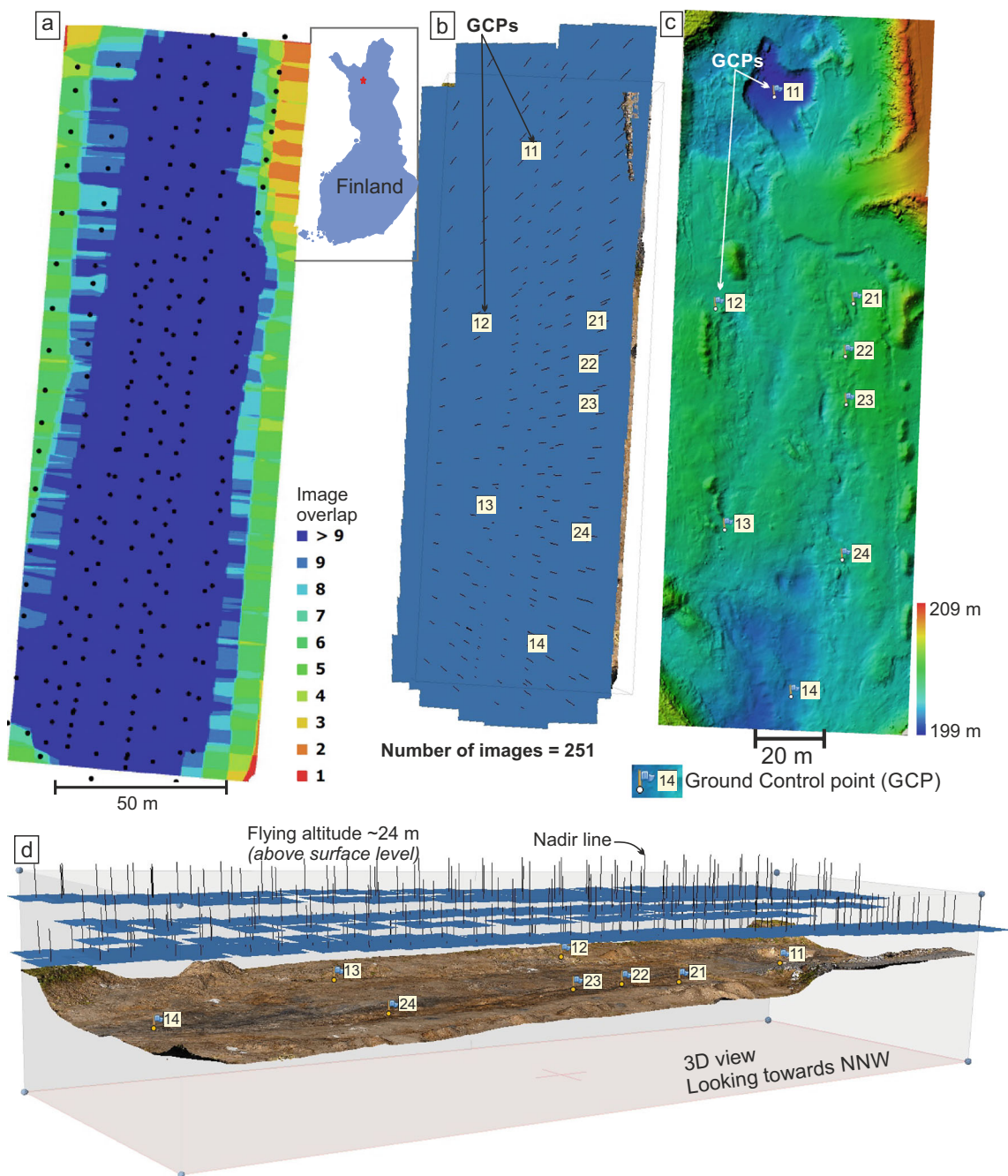
Fig. 2 **a** SFM-MVS-based approach using UVA. Photo alignment and the graphical representation of the image overlap in a "reference" mode are shown. Two hundred fifty-one georeferenced images were taken at an altitude of about 24 m from the ground surface. **b** The blue squares with nadir (center) lines represent camera positions and orientations detected by the PhotoScan software. Eight ground control points (GCPs) were used for georeferencing during the Photoscan workflow and are shown in yellow boxes and blue flags. **c** Digital elevation model (DEM) of the Etelä pit showing elevation gradient from blue (low) to red (high). Blue flags indicate locations of the GCPs in yellow boxes. **d** 3D view of the model in a perspective view

points for the dense point cloud. A DEM (3.52 cm/pixel) was generated with a point density of 806 points/m^2 (Fig. 2c). Finally, an orthomosaic image at 8.8 mm/pixel was produced, which strengthened the geological map features (Fig. 3). Root-mean-square error (RMSE) calculated from eight GCPs are 3.6 cm in the X direction (easting), 6.2 cm in the Y direction (northing), and 2.0 in the Z direction (vertical).

Further technical details and survey procedures on mapping the open pit using the UAV-based SfM-MVS approach were recently published by Sayab et al. (2018).

A detailed geological map of the Etelä pit was prepared and shows the main lithological components (Fig. 3a). The map was integrated with the ultra-high-resolution aerial image (Fig. 3b). Structural data collected from 22 locations within
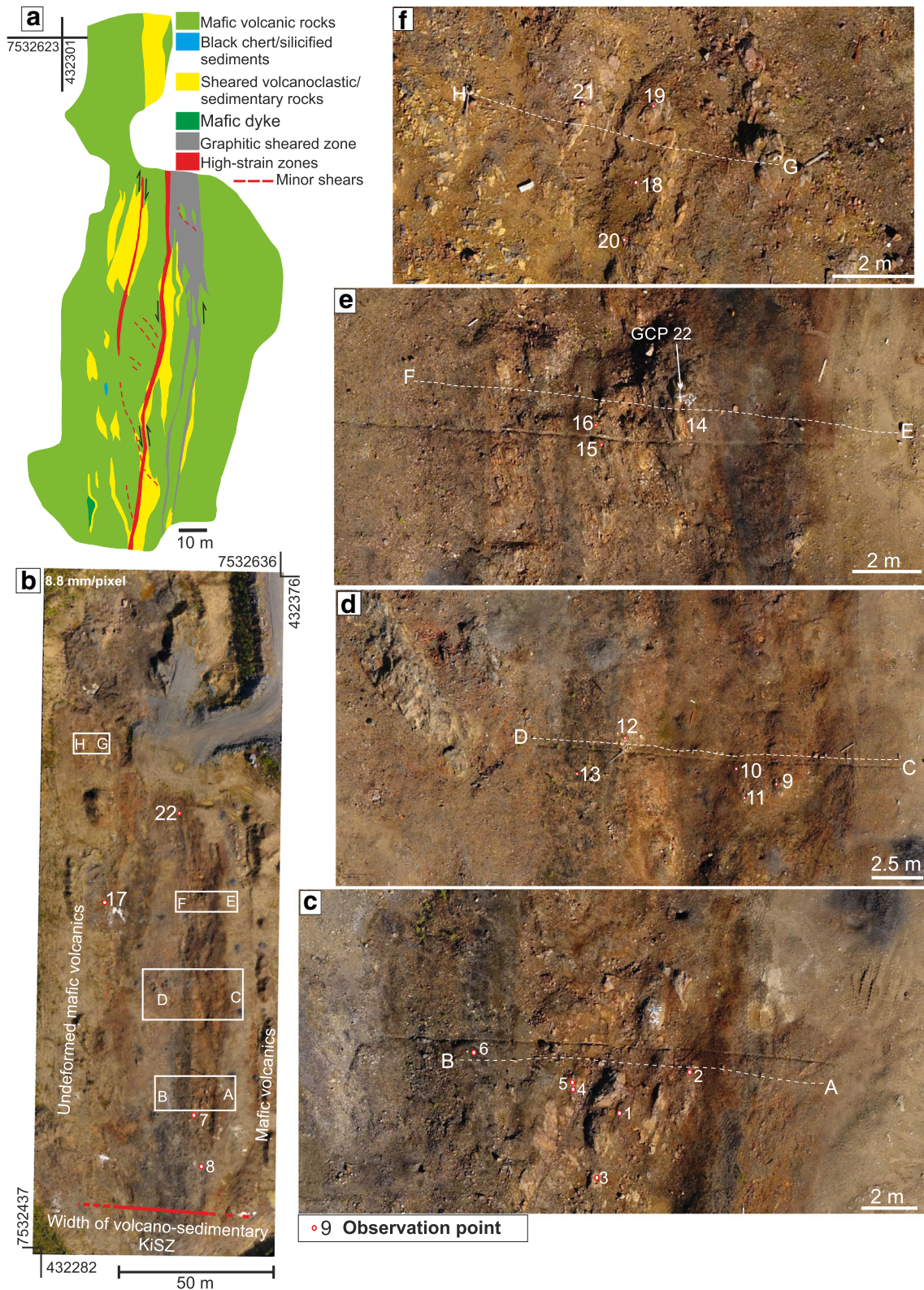
Fig. 3 **a** Geological map of the Etelä pit showing the main lithological units. **b** Orthorectified image of the Etelä pit showing part of the Kiistala shear zone (KiSZ). The resolution of the image is 8.8 mm/pixel. White boxes are enlarged in **c** to **f**. Numbers from 1 to 22 represent field locations. KiSZ (Kiistala Shear Zone) is used in this and subsequent figures

the pit are shown on the aerial image (Fig. 3b–f). For statistical analysis, our structural data were grouped into blocks AB, CD, EF, and GH, although some points fall outside these blocks including 7, 8, 17, and 22 (Fig. 3).

X-ray computed micro-tomography 3D data acquisition and processing

X-ray computed micro-tomography (XCT) allows 3D visualization, mineral quantification, and metamorphic fabric analysis down to the micrometer scale (Sayab et al. 2015, 2017; Aerden and Sayab 2017; Suuronen and Sayab 2018). Because the XCT technique differentiates different minerals based on their contrasting densities, the method is particularly useful for analyzing the distribution of sulfide minerals within their host rock (Kyle and Ketcham 2015; Sayab et al. 2016).

Two oriented samples were analyzed using the recently installed GE phoenix v|tome|x s micro-tomography instrument of the Geological Survey of Finland at Espoo. For these samples, different scanning configurations were used because of the different sizes of the samples. The instrument is equipped with a 240-kV directional microfocus tube and a 180-kV transmission nanofocus tube with a large high-contrast (2024 × 2024 pixel) flat-panel detector GE DXR250. Acquisition and reconstruction were performed with phoenix datos|x module package. All the XCT data were processed using the PerGeos software developed by ThermoFisher Scientific (https://www.fei.com/) for visualization, segmentation, and quantitative measurements.

The sample Kittilä-01 was scanned with the microfocus tube in two parts due to the relatively large sample size (~ 15 × 8 × 10 cm), lasting about 2.8 h each, resulting in a total scan time of about 5.5 h. The instrument was operated with an acceleration voltage of 220 kV and a tube current of 250 μA. The X-ray radiation was filtered with 1.0 mm of Cu and 0.5 mm Al to reduce beam hardening and enhance contrast. Two thousand five hundred projections per 360° were acquired in a single scan resulting in a total of 5000 projections for the two scans with a 1000-ms exposure time and each image an average over three exposures. After each angle step, the detector waited for a single exposure time for the afterglow to stabilize. Based on these configurations, the resulting 3D volume has a voxel size of 65 μm. In the case of sample Kittilä-02 (14 × 4.5 × 3 cm), the sample was scanned with the microfocus tube in two parts, each lasting about 3 h, resulting in a total scan time of about 6 h. The sample was scanned at 200 kV and 200 μA. The X-ray radiation was filtered with 0.5 mm of Cu and 0.5 mm Al plates. A total of 5400 projections were acquired with a 1000-ms exposure time and each image an average over three exposures. The scanning parameters yielded a voxel size of 40 μm. 3D microstructural interpretations of the each sample are presented below.

Seismic profiles

As part of the High-Resolution Reflection Seismics for Ore Exploration 2007–2010 (HIRE) project, a total of 133.8-km 2D reflection seismic profiles were acquired from the Suurikuusikko and adjacent Petäjäselkä areas (Kukkonen et al. 2009). The HIRE data, including the Geological Survey of Finland geophysical (airborne magnetic, electromagnetic, and ground gravimetric) and geological data, was used in generating a unified 3D structural model of the area (Niiranen 2015). In this study, we used the roughly east-west running Suurikuusikko and Petäjäselkä reflection seismic profiles (Fig. 1b) to decipher the subsurface structural geometry of the KiSZ (see below).

Field observations

Description of mesostructures

The shear zone controlling the location of the orebody at the Etelä pit is the part of the KiSZ. The shear zone is characterized by ductile to brittle deformation transitions manifested by a penetrative foliation showing opposite shear senses, small-scale rootless intrafolial folds, mylonite, slickensides, and Riedel veins and fractures, recording a complex deformation history. The shear zone is hosted by highly altered volcanic and sedimentary rocks (Fig. 3a). Regional chloritization of host rocks is ubiquitous and indicates metamorphic conditions up to greenschist facies. Relatively undeformed tholeitic volcanic rocks occur beyond the shear zone boundaries. The overall width of the shear zone is not more than 50 m in the Etelä pit but varies laterally likely due to variable partitioning of deformation.

Shear zone foliation S_R

S_R is a penetrative, reactivated shear foliation that developed along the shear zone. It is subvertical and strikes from NNE-SSW to NNW-SSE. Box G–H on Figs. 3f and 4a and b shows its progressive development from low- to high-strain. At location 21 (Figs. 3f and 4a), the volcanic rocks show asymmetric crenulations with the dextral shear component. The foliation grades into a mylonitic fabric (Sm-1; Fig. 4b) show S-C and felsic σ-type kinematic indicators with a dextral sense of movement. S_R is coarsely-developed in some competent pockets (Fig. 4c), especially at the eastern and western margins of the shear zone. At location 17 (Fig. 3b), S_R is overprinted by sinistral NNW-SSE striking shear bands (Fig. 5).

Mylonitic band

A dark gray ca. 2-m thick, NNW-SSE striking, subvertical mylonite zone (Sm-2) occurs in the middle of the shear zone, from location 6 to 16 through location 13 (Fig. 3). At all these locations, the mylonite preserves excellent asymmetric shear
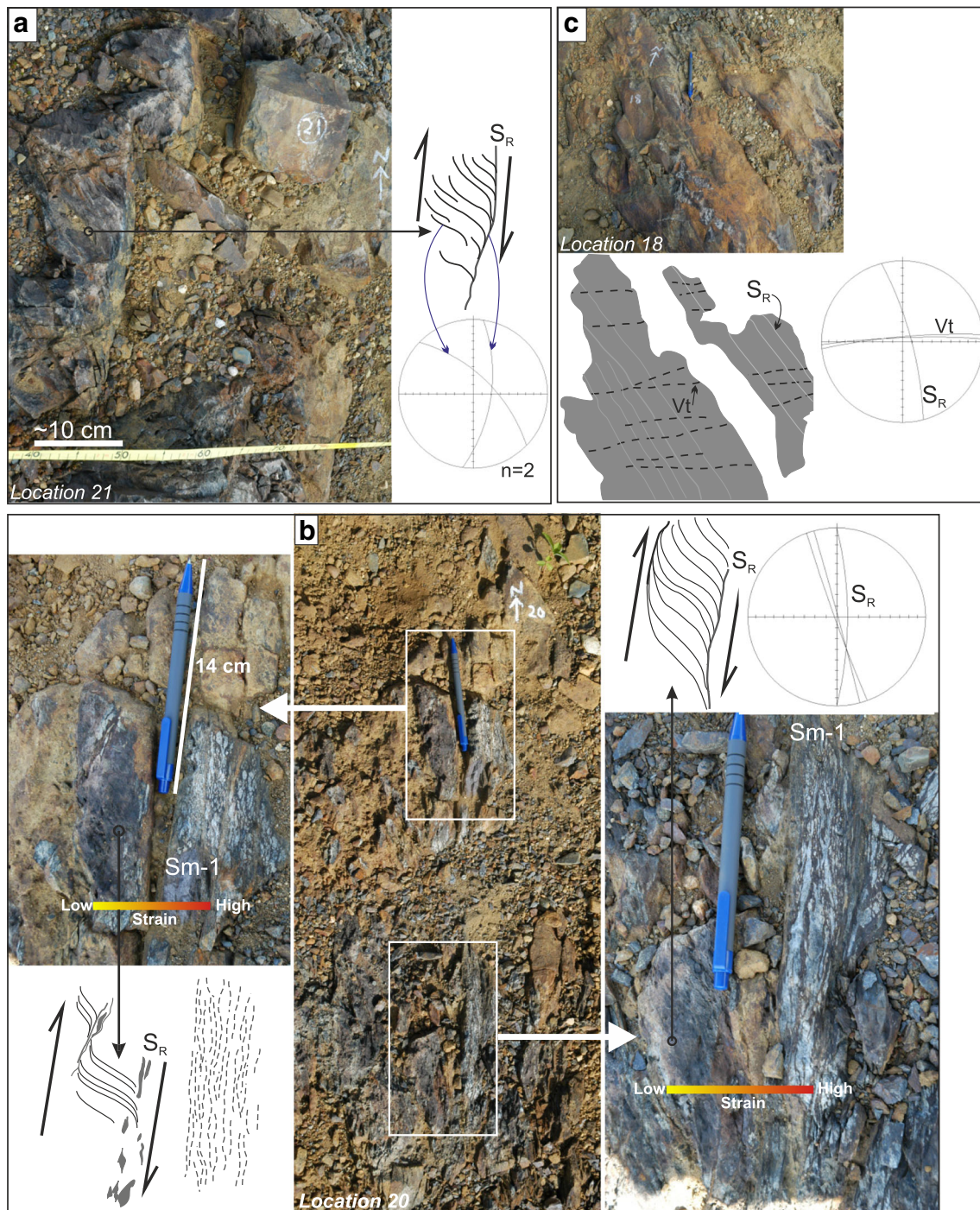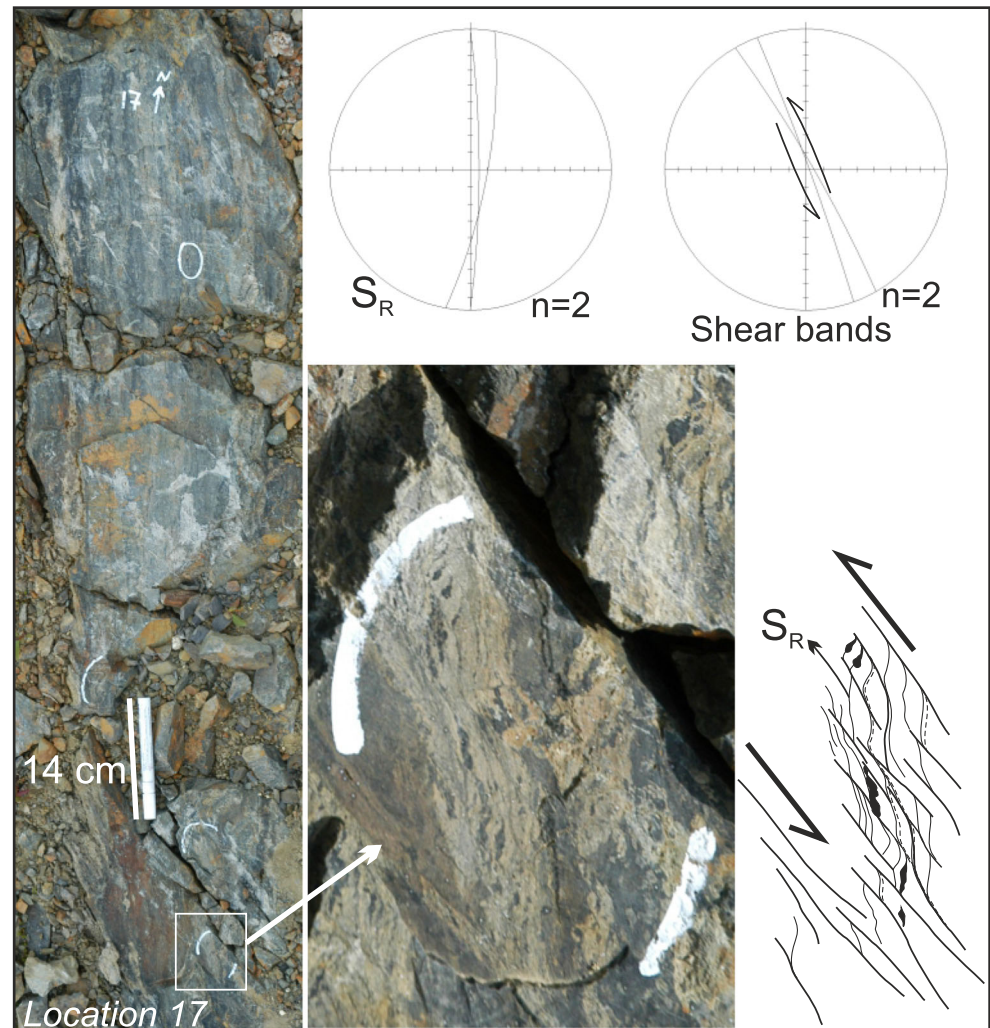
Fig. 4 a Field location 21 showing prominent dextral movement preserved within the volcanic rocks of the KiSZ. The shear foliation is marked by S_R. **b** Location 20 showing low- to high-strained parts (stage 3, 4, to 6 of crenulation cleavage development) of the shear zone from west to east, respectively, in enlarged photographs. The high-strain zone is characterized by mylonitic fabric (Sm-1). **c** S_R at location 18 is spaced and cut by tension veins, Vt. Structural measurements are shown as lower hemisphere equal-area stereographic plots

sense indicators in the form of σ- and δ-type felic clasts and S-C fabrics consistently showing a sinistral shear sense (Fig. 6), thus opposite to the shear sense noted along S_R and Sm-1. These clasts are probably derived from pyroclastic material embedded in the mafic host rock. Because of the relatively flat outcrop surface, the plunge of the mylonitic fabric was difficult to

measure, so this was done in an oriented sample taken for this purpose at location 6 (see below). The difference in the shear sense in Sm-1 and Sm-2 indicates that both were affected by two discrete events, and examined below. Nevertheless, the S_R foliation both in the volcanic and graphitic rocks, away from the Sm-1 and Sm-2, is characterized by penetrative shear foliation.

Folds

Relict, less than meter scale tight to isoclinal folds were observed
in relatively competent volcanic rocks (Online Resource 1 and
observation points on Fig. 3b and d). The limbs of these folds
were dislocated and untraceable across the shear bands.
However, the fold axes are moderately to steeply plunging dom-
inantly towards the south, SSE, and in one instance NNW. A
faint foliation parallel to folded bedding layers and thin quartz-
calcite (mm scale) veins constitutes S1 (Online Resource 1a, c).
These folds are cut by a penetrative, axial planar cleavage, which
is steeply dipping and NNW-SSE striking. We interpret this fo-
liation as S_R described above because of its repeated reactivation
during a polyphase evolution of the shear zone as is shown
below. Fold axes associated with the intersection between S1
and S_R planes are accordingly labeled F^1_R.

Lineation

Well-developed SSW trending and moderately to shallow
plunging ridge-in-groove type slickenside striations (Means

1987) are exposed in the southern part of the pit (location 8
on Figs. 3b and 7a, b). The lineation is defined by mineral
fibers and is associated with rough congruous "step" struc-
tures (Lin and Williams 1992) contained within the shear sur-
face (Fig. 7a). The "smoothness-roughness" criterion of
(Billings 1954) indicates a dextral shear sense. The lineation
overprints a moderately to steeply NW to NNW-plunging
mineral stretching lineation that is designated as L_1 (Fig.
7b). Therefore, we label the pronounced slickenside lineation
as L_2.

Veins and fractures

Several vein sets and fractures can be distinguished in the
shear zone based on their mode, orientation, and cross-
cutting relationships. Small layer-parallel quartz veinlets
deformed by rootless intrafolial folds are the earliest veins.
These veinlets are parallel to the folded layers; hence, we
label Vf (Online Resource 1a,c). They are overprinted by
S_R.
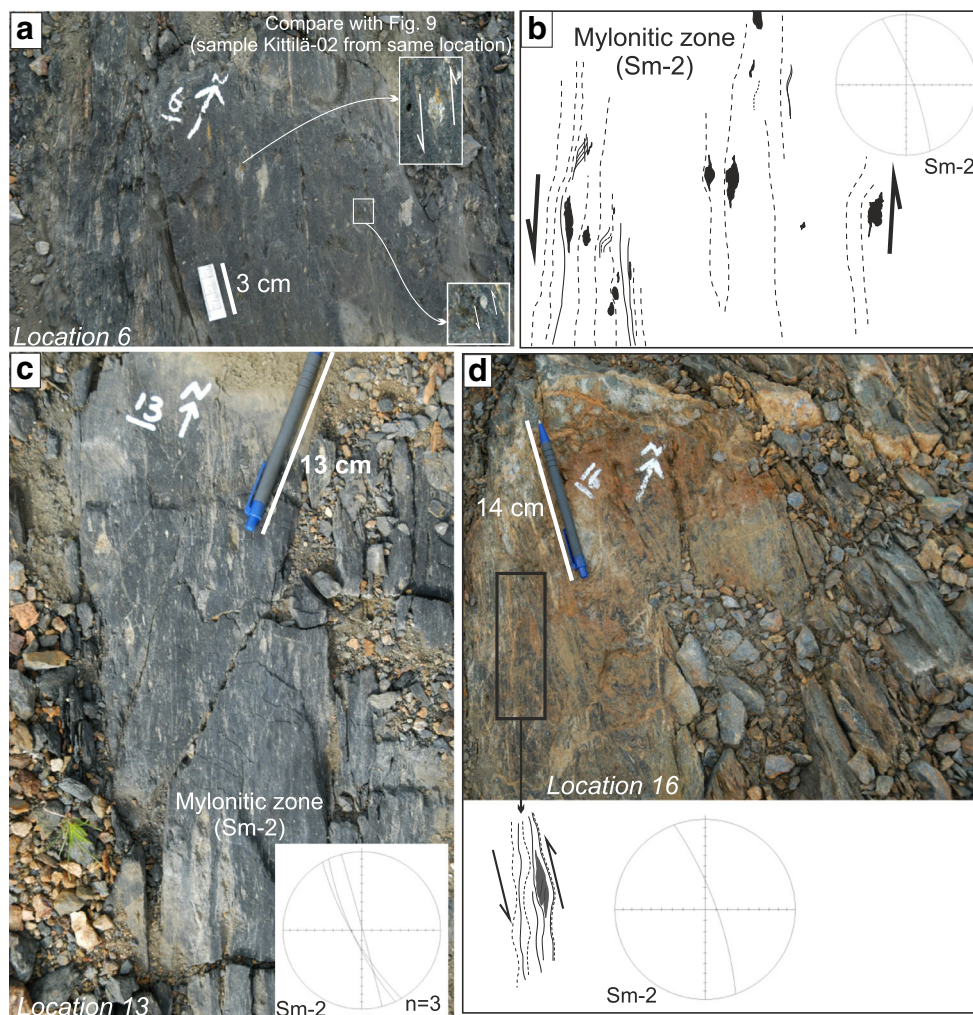
A younger vein array cuts S_R at angles of ~40–70° counterclockwise from the strike of this shear cleavage. They are developed along the full length of the shear zone (Figs. 4c and 7c–e and Online Resource 1d) but are absent in the mylonitic zone with Sm-2 foliation. The veins are planar or occasionally sigmoidal and rarely arranged in an en-échelon pattern. Their average strike is ESE-WNW and they have steep dips (Figs. 7c–e). The veins were formed by tension normal to the vein walls as indicated by blocky crystals of sulfides, and hence labeled as Vt.

The third set of NNE-SSW to NE-SW trending thin veins strike ~30° to 55° clockwise from the trace of S_R are spatially associated with Vt veins. Since they exhibit both opening and shearing components, we refer to them as hybrid veins and label them Vh-1 (Online Resource 1b and Fig. 7c–e). Both Vt and Vh-1 intersect rather than offset each other (Fig. 7d, e). A less prominent NNW-SSE trending set of thin veins, oriented 20–30° counterclockwise to the trace of the S_R, also show both shearing and opening modes and are called Vh-2. The Vh-2 cross cuts the Vh-1 set without any noticeable offset. The paragenetic sequences of each vein set are detailed further below.

Microstructures—X-ray computed micro-tomography

Sample Kittilä-01

The sample Kittilä-01 from location 01 (Fig. 3c) was selected to study the microstructures of sulfide-bearing versus sulfide-absent parts of the shear zone. The outcrop at this location is composed of fine-grained altered basic volcanic rocks. Planar to anastomosing thin sulfide, seams occur disseminated along the penetrative schistosity, S_R (cf. Figure 8 and Online Resource 2a). The S_R is cut by younger sulfide-bearing veins (Online Resource 2).

The 3D XCT image of the sample was digitally cut into 8 vertical slices perpendicular to the main schistosity (S_R), 4 vertical slices parallel to the schistosity (S_R), and 3 horizontal slices (Fig. 8a). The XCT data revealed a contrast in density and different spatial distribution of sulfides in dark- and light-colored zones that can be distinguished with the naked eye (Fig. 8a–f). The light color sheared zone appears as a homogeneous dark layer in the XCT image due to its lower-density devoid of any sulfides in all digital sections (Fig. 8). This zone
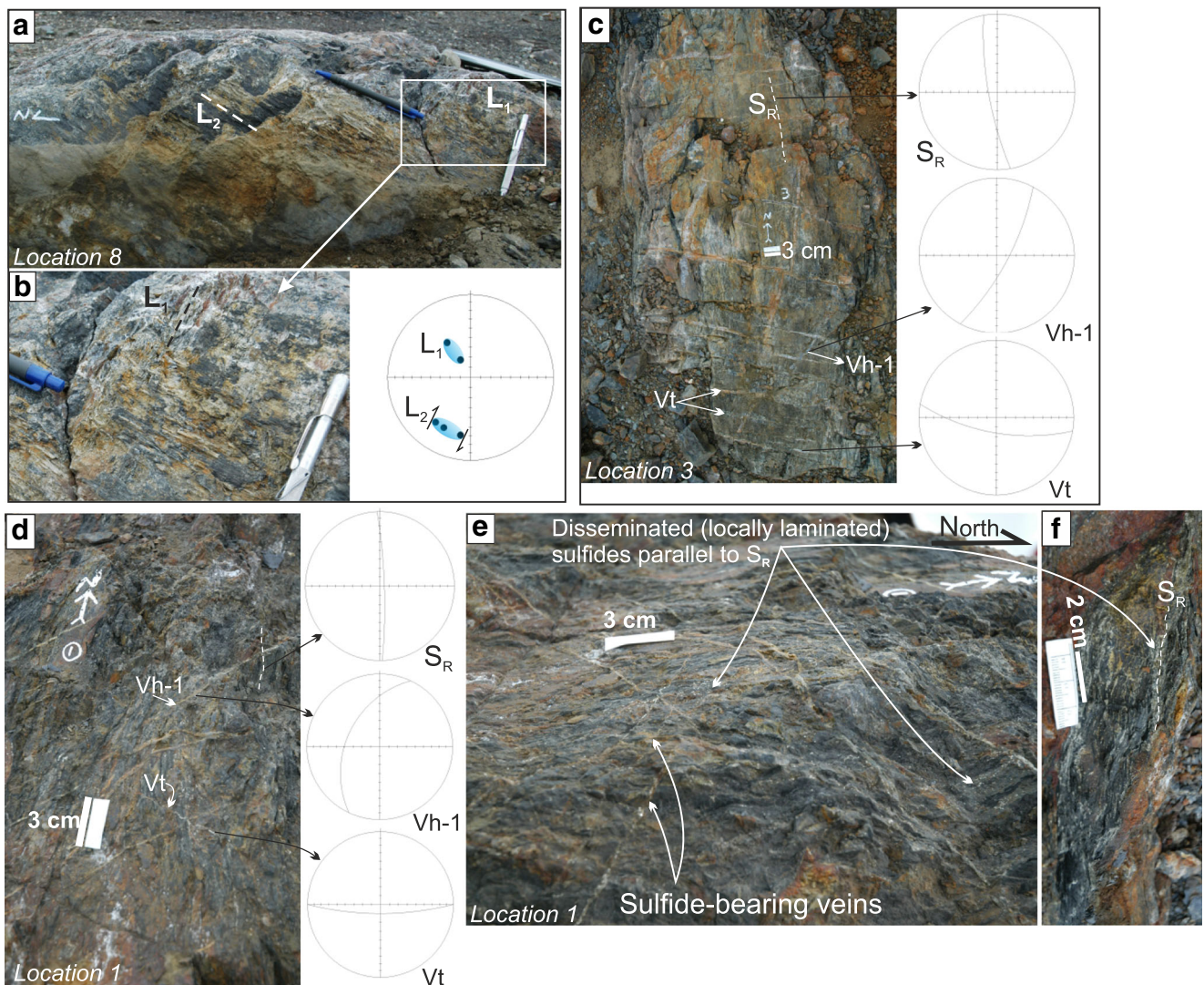
Fig. 7 **a** Field photograph showing L$_2$ slickenside striae moderately to shallow plunging towards the S-SW. **b** Relic L$_1$ mineral lineation, moderately to steeply plunging towards the NNW. **c** Geometrical relationship showing the orientations of S$_R$ foliation, Vt, and Vh-1 veins. Note that both Vt and Vh-1 veins cut across the S$_R$ foliation. **d, e** Location 1 showing strike orientations of S$_R$, Vt and Vh-1 as seen at location 3. **f** Enlarge view of a part of location 1 displaying sulfide mineral seams along anastomosing S$_R$ foliation. Structural measurements are shown as lower hemisphere equal-area stereographic plots

contains relatively large clasts surrounded by a fine-grained matrix. In contrast, the dark color sulfide-bearing sheared zone appears as a heterogeneous light-colored domain in the XCT image, due to a higher density and define a semi-massive distribution of sulfides localized along the penetrative schistosity (Fig. 8d, f), as already noticed in outcrop (cf. Figures 7d-f and 8b). Moreover, the sulfide-bearing zones further exhibit finely disseminated bright arsenopyrite (prismatic to acicular) and pyrite (cubic) grains within veins and the matrix, also directly visible in hand specimen. Sayab et al. (2016) studied this sulfide mineralization at ultra-high resolution using synchrotron X-ray nanotomography and determined the 3D textural setting of gold inclusions inside arsenopyrite (see below).

The sample further contains a set of planar Vt veins (Online Resource 2b, c) that cross-cut the sulfide-bearing foliation as is manifested by high-density sulfides (red colored veins in Online Resource 2b, c). Another less prominent vein set with an average orientation of N 030–040°, and attributed to Vh-1, also cuts the main matrix foliation (S$_R$) but is devoid of sulfide mineral grains (Online Resource 2b). The Vh-1 veins are visible on the hand specimen, but cannot be seen in the XCT image due to their low density (they are composed of quartz or calcite).

Within the sulfide-bearing zone, in low-strain domains of S$_R$, the N-S sections of the sample reveal a tight to isoclinal recumbent fold verging towards the north (Fig. 8a and Online Resource 3). Through virtual scrolling along the vertical XCT sections, the orientation of the axial planar cleavage and fold axis could be determined to be sub-horizontal and E-W trending, respectively (Online Resource 3b, c, d). Sulfide mineralization in this
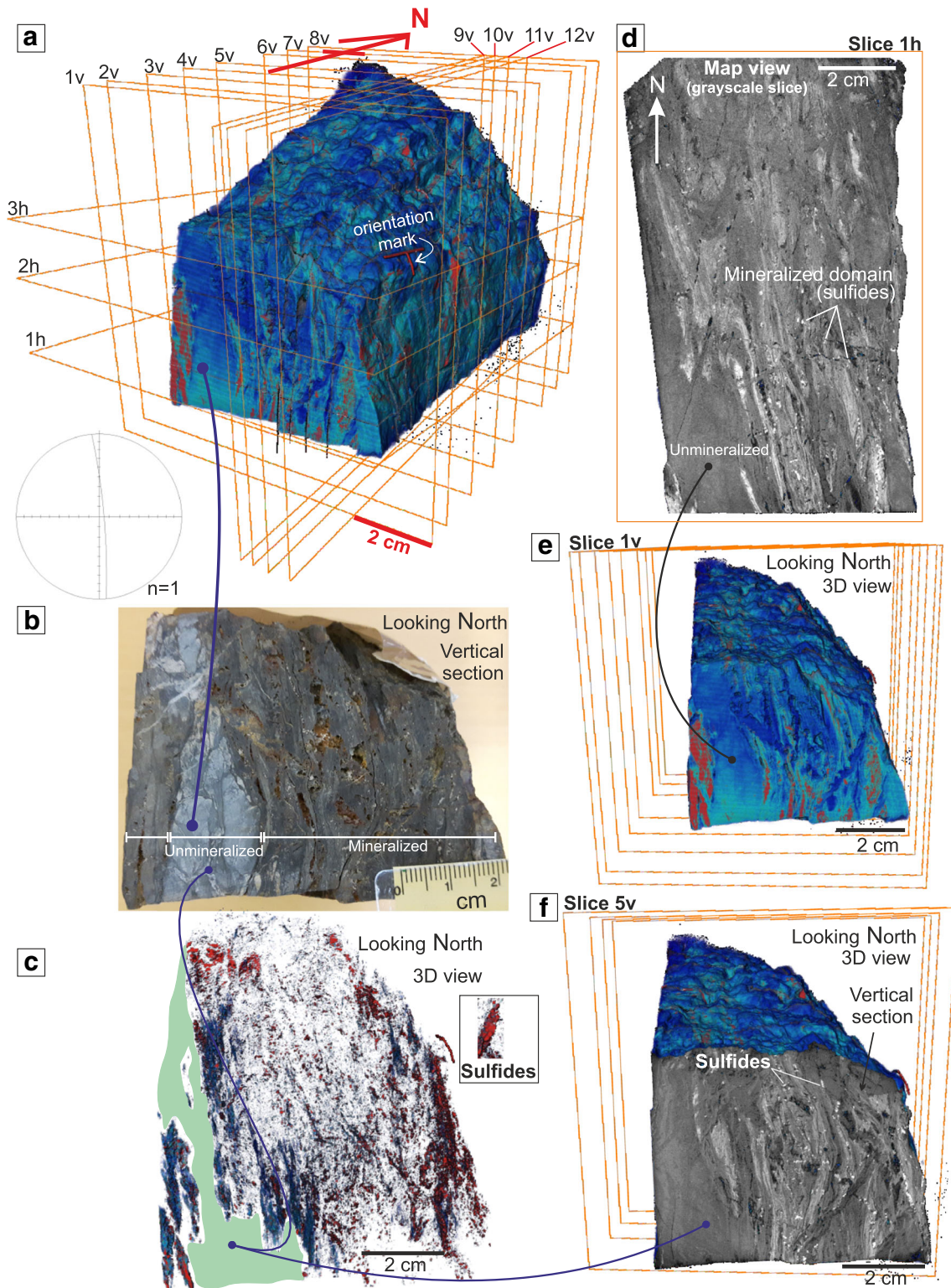
Fig. 8 Different three-dimensional (3D) representations of XCT data from oriented sample Kittilä-01. **a** 3D image showing the positions of vertical (v) and horizontal (h) slices across the sample. Lower hemisphere, equal-area stereographic plot depicts the spatial orientation of the sample. **b** Vertical view of the hand specimen oriented in such a way to compare the sulfide-bearing (dark color) vs. sulfide-absent (light color) zones. **c** 3D image oriented exactly the same as shown in panel **b**. No sulfides were detected in the lighter color zone marked as green. The rock matrix is rendered transparent. **d** 2D horizontal slice (1 h) showing the sulfide-bearing vs. sulfide-absent zones in a greyscale image. **e** and **f** comparison of the same two zones in different vertical profiles (1v and 5v)

recumbent fold is localized along both the folded layering and the axial planar cleavage (Online Resource 3b, c).

Sample Kittilä-02

The sample Kittilä-02 was collected from the mylonite zone (location 06; Fig. 3c) to determine the plunge direction of the mylonitic shear and further study its kinematics. This can be deduced from the long axes of porphyroclasts with respect to the mylonitic foliation (Bell and Johnson 1992). No sulfide-bearing veins occur in this sample. Sulfides exclusively occur as rims around deformed lithoclasts (Fig. 9a–f).

Asymmetric porphyroclasts show a sinistral sense of movement in horizontal sections (Fig. 9a,d). To determine the plunge of the shearing direction, several digital sections were examined some of which are shown in Fig. 9b. The volume-rendered 3D image, while looking downwards, shows that the long axes of porphyroclasts lie within the mylonitic foliation (Fig. 9c). Side views of the same 3D rendered image shows their shallow plunge (0–23°) towards the NNW (Fig. 9c–g) defining a stretching lineation. Most of the porphyroclasts are mantled by sulfides as can be seen both by visual inspection and in the XCT images (Fig. 9a–f). These sulfide-mantled porphyroclasts are interpreted as primary fragments of sedimentary or volcaniclastic origin.

Kinematic interpretation

The KiSZ records multiple episodes of structurally controlled hydrothermal activity between ca. 1.92 and 1.77 Ga (Molnár et al. 2018). In this study, we have documented several generations of exquisitely preserved (micro) structures in the Etelä pit, which is part of the KiSZ. The structural sequence is obscured by repeated reactivation of this shear zone but has been resolved herein by a detailed study of structures and fabrics in outcrop integrated with X-ray tomography of oriented hand specimen (see below). Online Resource 4 summarizes the structural data collected for the different phases of deformation recognized.

Relative timing of dextral versus sinistral movement

NNW-SSE trending shear bands at location 17 (Fig. 5) exhibit the same sinistral movement and orientation as the mylonite zone whose main fabric is Sm-2 (locations 6, 13, and 16; Figs. 3 and 6). These shear bands overprint N-S and NNE-SSW striking S_R-foliated volcanic rocks exposed in the margin of the KiSZ. Locations 20 and 21, which are longitudinally well aligned with location 17 (Fig. 3), preserve variably developed S_R. With reference to the six stages of crenulation cleavage development described by Bell and Rubenach (1983), S_R at location 21 reaches stage 3 (moderately differentiated crenulation cleavage), whereas stages 4 (strongly differentiated) to

6 (completely transposed) are observed at location 20 (Fig. 4b). Stage 6 at location 20 corresponds to the mylonitic foliation (Sm-1), hence indicating a gradual increase of (shear) strain from west (stages 3 to 4) to east (stage 6). S_R at location 17 represents stage 6 of crenulation-foliation development. At locations 20 and 21, a dextral shear sense is indicated by crenulation asymmetry or porphyroclasts. These relationships suggest that the sinistral strike-slip movement recorded in a 2-m wide dark mylonitic band in the middle of the shear zone by mylonitic foliation Sm-2 is younger than the dextral Sm-1, and recorded in volcanic rocks closer to its margins. Thus, a narrow highly strained mylonitic zone (Sm-2) accommodated a sinistral strike-slip overprint that left the foliated volcanic rocks (Sm-1) near the margins of the shear zone unaffected. Strain softening during dextral shearing may account for the later strong partitioning of sinistral shearing in the finer-grained central part of the pre-existing shear zone (Bell 2010), whereas closer to the margins of the shear zone the rocks were relatively strong and escaped the sinistral shearing.

Two oppositely plunging mineral lineations, L_1 and L_2, have been identified at location 8 (Figs. 3b and 7a, b). L_2 lineation is characterized by well-defined, ridge-in-groove, slickenside striae, which is shallowly plunging to the SSW and has a distinct dextral movement. Such slickenside striae have been found in ductilely deformed rocks (Burg and Wilson 1988; Lin and Williams 1992), and therefore, we interpret that these mineral lineations (L_2) as being related to the dextral shear observed at locations 20 and 21 (Fig. 3). The shear sense along the early, steeply plunging, mineral stretching lineation (L_1) cannot be deduced; however, the orientation of this lineation is significant in terms of regional tectonics as discussed below.

Apart from the opposite shear senses along Sm-1 and Sm-2 (dextral versus sinistral), the lineation defined by porphyroclast long axes associated with Sm-2 (Fig. 9f, g) plunges gently NNW, whereas L_2 (location 8) associated with distinct dextral shearing plunges SSW. These differences imply that there were two different mylonite-forming events. Sm-2 is associated with sinistral shearing, post-dates Sm-1 and S_R, and is practically devoid of sulfide mineralization as seen in sample Kittilä-02. Sulfide-bearing clasts contained in this sample are interpreted to represent low-strain pods preserving either Sm-1 or S_R, whereas the sulfide-absent band in sample Kittilä-01, which cross-cuts mineralized (sulfide bearing) S_R, corresponds to Sm-2. However, the Sm-2 shear re-oriented the plunge direction of the sulfide-bearing lenses as seen in the case of lithoclasts (Fig. 9f, g).

Origin of early folds

The tectonic significance of the rootless intrafolial folds (Online Resource 1) whose limbs are truncated by S_R is difficult to interpret. Because they are moderately to steeply
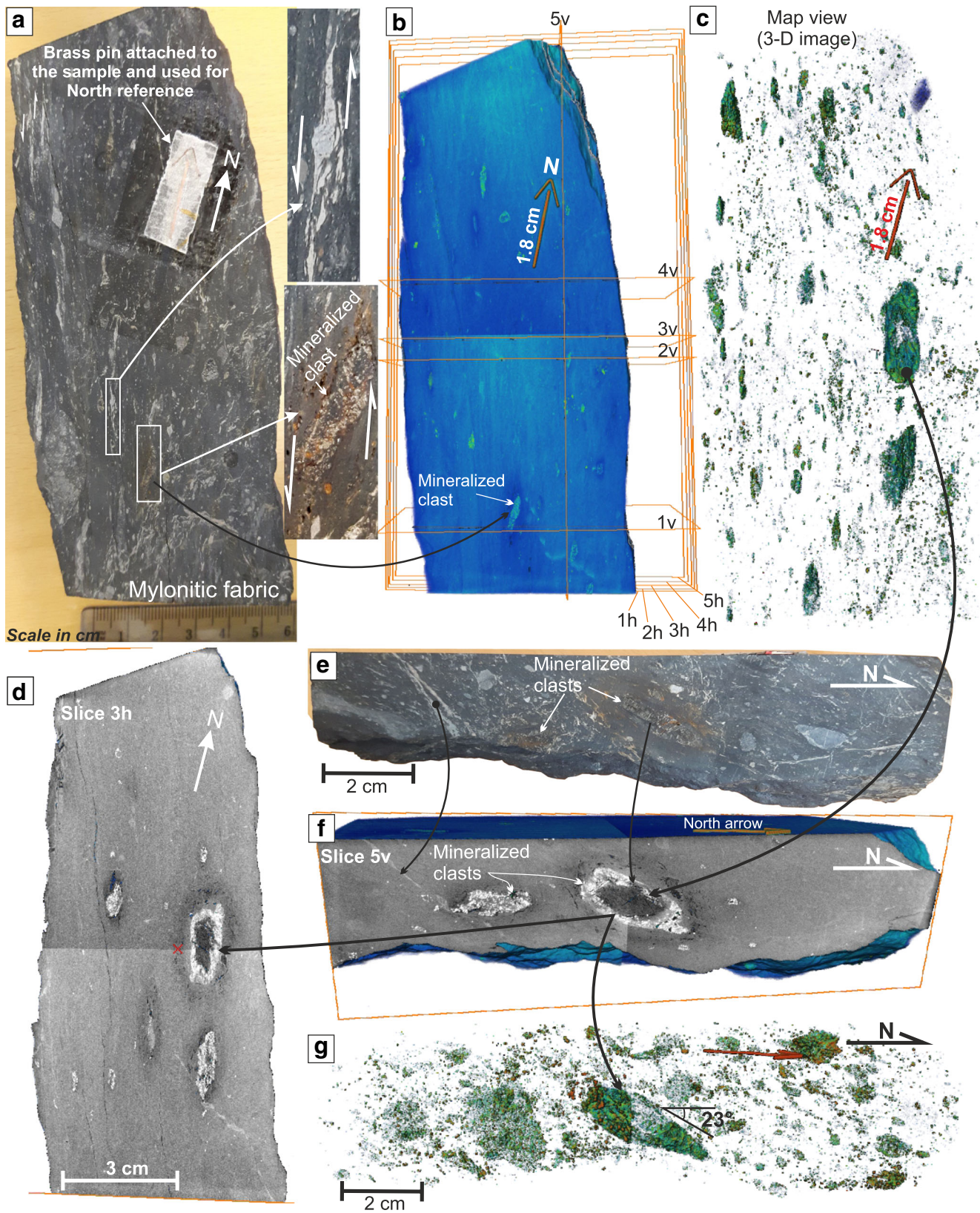
plunging towards the south and SSE, close to the plunge of L_2, it appears that they either formed synchronously with or pre-date S_R (Sm-1) and thus experienced dextral shearing.

Alternatively, these folds were originally plunging towards the NNW, as noted in one instance (Online Resource 4), sub-parallel to L_1, and were later rotated due to the dextral

Fig. 9 Different 3D images of XCT data from an oriented sample Kittilä-02. **a** Hand specimen showing dark-gray mylonitic fabric. The asymmetric porphyroclasts record distinct sinistral shear. Long axes of the sulfide-mantled prophyroclasts are parallel to the foliation; however, the rock matrix is devoid of any sulfide minerals. **b** 3D image showing the positions of vertical (v) and horizontal (h) slices around the sample. **c** Rendered XCT image showing preferred orientation of sulfide-rimmed clasts. **d** Greyscale XCT slice (map view) showing lithoclasts rimmed by sulfides (bright) masses. **e, f** The XCT imaging helped to find the largest clast preserved within the sample and dissected along slice number 5v (see panel **b**). **g** 3D XCT image where the rock matrix is rendered transparent. The long axes of the porphyroclasts are shallowly (ca. 23°) plunging towards the N
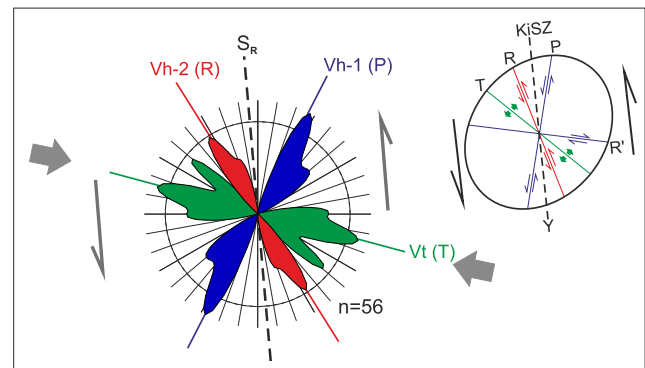

Fig. 10 Map view geometrical distribution of Vt, Vh-1, and Vh-2 with respect to North. Rose plot showing the relationship between the Vt, Vh-1, and Vh-2 and follow the sinistral strike-slip strain regime (e.g., Bartlett et al. 1981)

movement towards the south and SSE, sub-parallel to the direction of L_2. However, relic L_1 and NNW-plunging folds were not rotated and unaffected by the dextral shearing mainly due to deformation partitioning (Bell 2010). The axes of regional-scale folds and their NNE-SSW striking axial traces exposed in the southern part of the KiSZ (Fig. 1a) suggest that they may have formed as drag folds during dextral shearing or were pre-existing.

Within a low-strain domain of S_R, sample Kittilä-01 preserves a recumbent, north verging, isoclinal fold with roughly E-W trending fold axis. This fold pre-dates the S_R foliation and, hence, the strike-slip regime of the KiSZ.

Veins and their paragenesis

Four geometrical types of veins and fractures have been recognized in outcrops and hand specimens: (1) Vf veinlets parallel to the folded layers in rootless intrafolial folds, (2) ESE-WNW striking Vt veins, (3) NNE-SSW and NE-SW striking Vh-1 hybrid veins, and (4) a NNW-SSE-striking Vh-2 hybrid veins. The Vf veins constitute the earliest vein set. The variable strike of Vt veins is due to their en-échelon and sigmoidal shape that progressively developed during shearing and shortening. The orientation of veins and fracture sets as a function of shear strain (Bartlett et al. 1981) suggests that the Vt veins formed as pure tension fractures (Fig. 10), while Vh-1 and Vh-2 could have formed synchronously as synthetic P and R fractures, respectively, in the sinistral strike-slip regime with a shortening component near-orthogonal to the Vt veins (Fig. 10). This sinistral shearing appears to have been produced during the continuation or waning stages of the Sm-2 regime.

Suurikuusikko and Petäjäselkä reflection seismic profiles

The east-west running seismic profiles of Suurikuusikko and Petäjäselkä exhibit a set of west-verging thrust faults and associated upright to inclined folding patterns (Fig. 11). The base of the Kittilä Suite acted as a detachment zone. Despite the steeply dipping geometry of the KiSZ at the surface, the subsurface seismic signatures mimic moderate dips towards

the east. Therefore, we interpret the KiSZ as a west-verging thrust splay, within a thrust system that roots into a detachment at the base of the Kittilä. The kinematics and relative timing between the strike-slip regime and thrusting phase of the KiSZ are further discussed below.

Discussion: Regional implications and timing of gold mineralization

In this study, we have integrated our field observations, UAV-based high-spatial-resolution aerial image of the Etelä pit, micro-tomography 3D analysis of selected rock samples, high-fidelity aeromagnetic and reflection seismic profiles to understand the kinematics of the KiSZ with emphasis on the Suurikuusikko gold deposit. Below, we discuss our findings and results in the light of previous studies and put forward a multi-stage tectonic model for the evolution of the KiSZ (Fig. 12).

D1 deformation

We interpret the KiSZ as part of a west-verging thrust system based on the high-resolution reflection seismic data. The steep nature of the KiSZ at the surface is due to the later strike-slip reactivation (Patison et al. 2007). Relic, L_1 stretching lineation plunges moderately to steeply NW to NNW and pre-dates the dextral shearing. We infer that the L_1 is attributable to an initial thrusting phase, D1, and characterized by E-W bulk shortening (ca. 1.92–1.91 Ga), consistent with the models of Nironen (2017) and Lahtinen et al. (2018) (Fig. 12a), who interpreted it as a consequence of the collision between the Norrbotten and Karelia lithospheric blocks. Most of the gold within the Suurikuusikko deposit is refractory and locked inside arseno-pyrite (73.2%) and pyrite (22.7%) (Kojonen and Johanson 1999). Rhenium-osmium (Re-Os) isochron dating of arseno-pyrite yielded a 1916 ± 16 Ma age for the mineralization (Wyche et al. 2015). This age is consistent with the early collisional phase proposed by Lahtinen et al. (2018).

Fig. 11 **a** Interpretation along the Suurikuusikko reflection seismic profile (A–B). The KiSZ (blue color thick dot line) is well imaged through this section. Traces of the form lines (solid white lines) are offset by the KiSZ. **b** Petäjäselkä reflection seismic profile (C–D) showing the geometry of the west-vergent thrust splays (blue color thick dot lines). Thrust-related folds are represented as white lines. The Kittilä base is marked by a west-dipping detachment zone. CMP, common midpoint
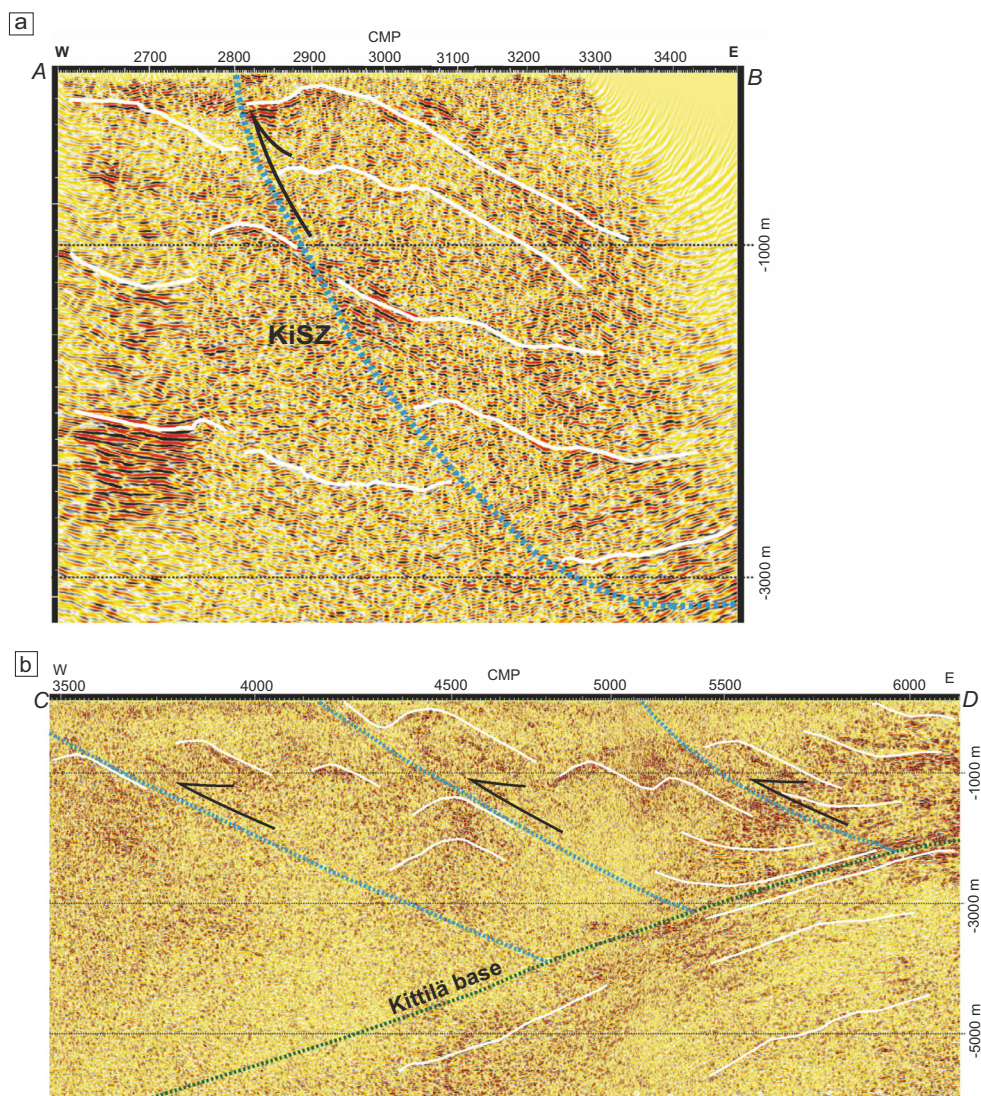
Sayab et al. (2016) analyzed individual arsenopyrite crystals from the main Suurikuusikko gold deposit in 3D, using synchrotron X-ray nanotomography. They found gold to be closely associated with rutile inclusions inside arsenopyrite crystals. Based on detailed 3D quantitative measurements (long, short, and medium axes) of rutile crystals, they recognized the preferred alignment of rutile inclusions inside arsenopyrite and suggested a structural control on rutile. They proposed that pre-existing rutile was formed by in-situ redistribution of the Ti content of mafic rock-forming minerals during thrusting when auriferous fluids were synchronously injected into the system. The 3D nano-textures imply that nano-grains of gold were precipitated along with the rutile in the first ore-forming phase (Sayab et al. 2016). The sulfide-bearing fluids crystallized either synchronously or late during the E-W bulk shortening phase trapping rutile along with the gold as inclusions. The lattice-bound or submicron-scale gold inclusions in arsenopyrite and pyrite reported by Kojonen and

Johanson (1999) and Wyche et al. (2015) may have formed during the same crystallization event. Thus, the KiSZ is a part of a D1 thrust system (E-W bulk shortening), and we further interpret that this early thrusting phase provided the first-order structural control on the localization of the Suurikuusikko gold deposit, given that the deposit is located on a ca. 20° bend in the KiSZ (cf. Figures 1 and 12a). These structural bends or jogs provide favorable sites for ore-forming fluid pathways of metamorphic origin (Groves et al. 2018).

Molnár et al. (2018) investigated the behavior of the Re-Os system in arsenopyrite at Iso-Kuotko. Their data did not define an isochron for deposition of early gold-bearing arsenopyrite, because of disturbance of the Re-Os system during subsequent fluid flow alteration events. Model calculations suggest that those overprinting events occurred at around ca. 1.88 Ga and 1.77 Ga corresponding to fluid flow events dated by monazite and xenotime.

Fig. 12 Synoptic tectonic model for the evolution of Kiistala shear zone (KiSZ). **a** D1 east-west bulk contraction and thrusting with the formation of Suurikuusikko and Iso-Kuotko gold deposits at the slight bends. **b** N-S shortening (D2), wherein strain was heterogeneously distributed at the regional scale (high magnitude on the eastern part of the CLGB as compared to the west). **c** NE-SW shortening switched the deformation regime from compression to transpression, hence, the kinematics of the KiSZ changed from dip- to strike-slip. **d** A near-orthogonal change in the regional stress regime from NE-SW to NW-SE flipped the kinematics of the KiSZ from dextral to sinistral (D4). **e** Finally, broadly E-W shortening (D5) marked the waning stages of deformation, where the localized dextral shearing at the Iso-Kuotko gold deposit caused veining and gold mineralization
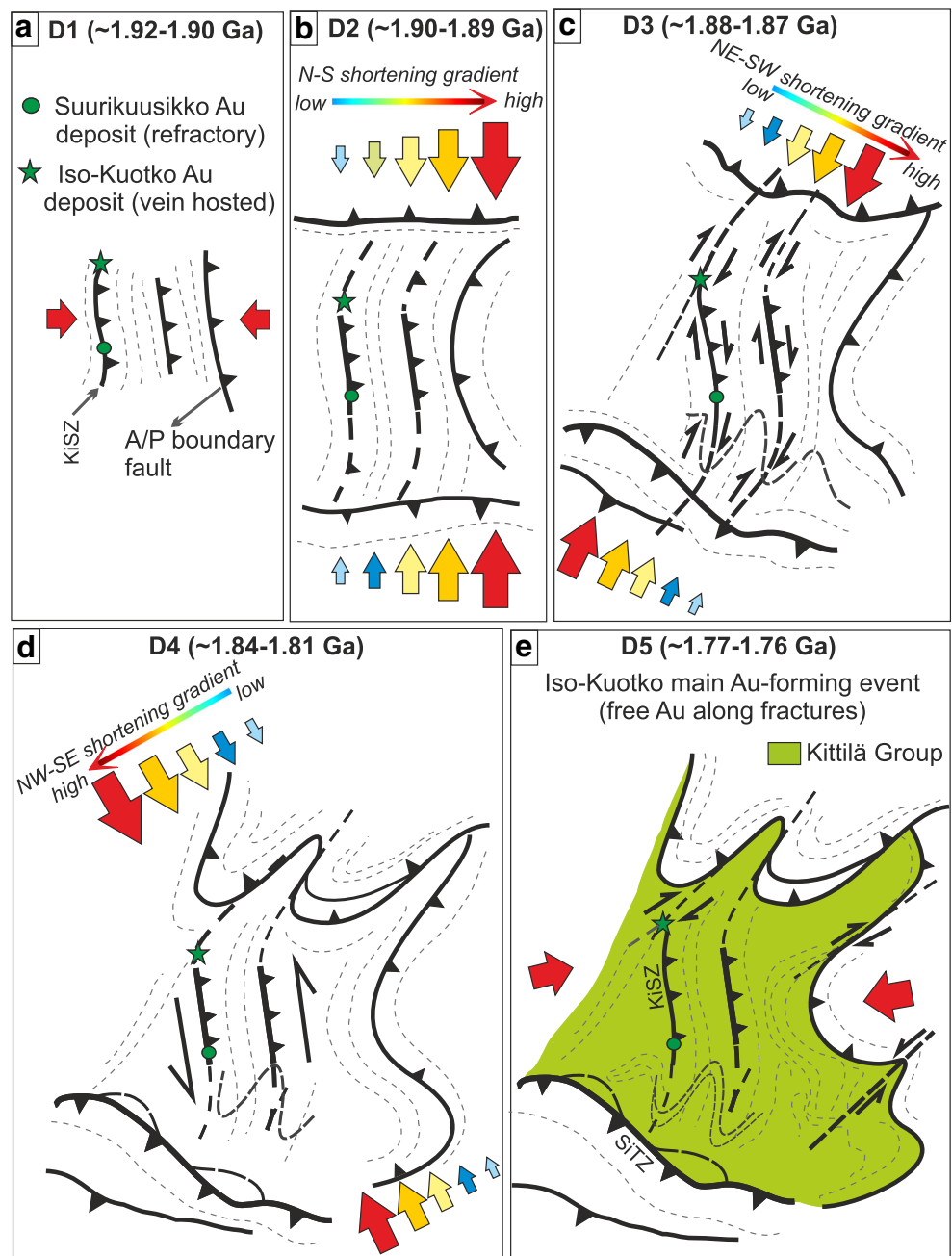
D2 deformation

The regional N-S shortening phase, attributed here to our D2 event, involved contemporaneous north- to NNE-directed and south- to SSW-directed thrusting along the southern and north-eastern boundaries of the CLGB, respectively, (Ward et al. 1989) as a result of the collision between the Lapland-Kola and Karelia lithospheric blocks (Nironen 2017). Age-wise, both Nironen (2017) and Lahtinen et al. (2018) placed this event between ca.1.90 and 1.89 Ga.

South- to SSW-directed thrusting is indicated by the juxta-position of the Lapland Granulite belt onto CLGB successions in the northeast, whereas the north- to NNE-directed thrusting is well defined along the Sirkka and Venejoki thrust zones in the south (Fig. 1). Map patterns suggest that the Sirkka thrust zone (SiTZ) truncates and, hence, post-dates the KiSZ. We assume that most of the strain during regional N-S shortening (D2, this study) was taken up along the southern and northern margins of the CLGB, and the only effect that we can infer, based on the aeromagnetic image, is the broad "S-shape" bending of the KiSZ (Fig. 12b). North verging, small-scale recumbent isoclinal fold, which was observed within the low-strain domain of S_R, in sample Kittilä-01, may reflect the remnant of D2 event. This event facilitated the

remobilization and precipitation of the sulfides along the axial planar cleavage (Online Resource 3b, c).

D3 deformation

Both Nironen (2017) and Lahtinen et al. (2018) proposed that after regional N-S shortening, a phase of NE-vergent contraction took place. Nironen (2017) includes the formation of N and NE trending shear zones in the CLGB in this event. We consider that due to the misaligned lateral shortening gradients (Fig. 12c), a dextral strike-slip regime commenced with the vertical axes rotation and caused slight inward bending of the northern and southern thrust zone boundaries (Johnston et al. 2013; Rosenbaum 2014). The dextral strike-slip shearing observed in volcanic rocks at the margin of the KiSZ, within the Etelä pit, is a result of this tectonic activity and we place this event within D3 (Fig. 12c), dated by Lahtinen et al. (2018) at ca. 1.88–1.87 Ga. The moderately SSE-plunging rootless isoclinal folds observed at locations 7, 9, and 10 can be interpreted as either drag folds formed during the same dextral shearing that is also indicated at the regional scale (Figs. 1 and 12c) or they were pre-D3 as explained above.

The occurrence of visible gold along some fractures within arsenopyrite has been previously reported (Sayab et al. 2016). During dextral shearing, invisible gold associated with rutile or lattice-bound might have exsolved from the arsenopyrite crystal structure and remobilized into secondary fractures during D3. The process is most likely arsenopyrite being more ductile than surrounding silicates taking up shear and dissolving (releasing) the gold.

The Iso-Kuotko gold deposit, further north from the Suurikuusikko gold deposit, is located at the bend of the KiSZ, where it swings from N-S towards the NW (Fig. 1). Molnár et al. (2018) dated the hydrothermal event at ca. 1.87–1.86 Ga. This period is consistent with our D3 event, where the tectonic setting switches from compression to transpression with the development of a jog at the Iso-Kuotko gold deposit (Fig. 12c).

D4 deformation

Deformation continued with a near-orthogonal switch of the regional stress regime from NE-SW to NW-SE, and such an orthogonal flip in stress directions is a common tectonic phenomenon in many orogenic belts (e.g., Deng et al. 2016; Sayab et al. 2017). This deformation event flipped the kinematics of the KiSZ from dextral to sinistral. We consider that the central mylonitic zone (Sm-2) in the KiSZ with sinistral sense of shear is a manifestation of this event. At the regional scale, this deformation phase played a major role in shaping the Central Lapland Granitoid Complex (Lahtinen et al. 2018), and we envisage that it was responsible for further bending of the thrust zones in the north and towards the eastern boundary (Fig. 12d).

Nironen (2017) situates this deformation event at ca. 1.84–1.83 Ga, similar to Lahtinen et al. (2018; ca. 1.84 to 1.81 Ga). Molnár et al. (2018) documented fluid flow events without gold mineralization along the KiSZ at the Iso-Kuotko deposit by U-Pb dating of hydrothermal xenotime.

No significant sulfide-bearing mineralization was found in the mylonite zones (Sm-2) probably due to shear strain controlled dissolution. Nevertheless, the Riedel geometry of some sulfide-bearing veins and fractures suggest that they may have formed in a sinistral environment outside, yet influenced by, the Sm-2 mylonite zone, during the waning stages of D4 sinistral shearing (Figs. 10 and 12d). In spite of the Vt veins being sulfidic (sample Kittilä-01), this event did not produce gold deposition, as noted at the Iso-Kuotko deposit (Molnár et al. 2018).

D5 deformation

In between the regional D4 and D5 events, an orogenic extension phase has been postulated at around ca. 1.80–1.77 Ga associated with the emplacement of granites (Nironen 2017; Lahtinen et al. 2018). D5 deformation around 1.77–1.76 Ga, is characterized by broadly E-W shortening (Fig. 12e), which at the Iso-Kuotko gold deposit produced localized dextral shearing and late-stage breccia veining and fractures (Patison 2007). Most of the gold ore (80%) is associated with free gold-bearing pyrrhotite-rich veins, wherein xenotime associated with visible gold yielded U-Pb ages of ca. 1.77–1.76 Ga (Molnár et al. 2018). The timing of gold mineralization at the Iso-Kuotko gold deposit is concordant with the late ductile to brittle transition related to the D5 deformation event.

Conclusions

The volcano-sedimentary rocks exposed in the Etelä pit allowed us to put together the kinematic history of the KiSZ. Various structural elements were examined at different scales keeping in mind the prolonged nature of the Svecofennian orogeny (ca. 1.92 to 1.76 Ga). We have shown five discrete, near-orthogonal deformation events for the tectonic evolution of the CLGB, wherein the geometry of the KiSZ evolved during each event. Our deformation scheme complements the previous work by Nironen (2017) and Lahtinen et al. (2018). Multiple near-orthogonal deformation and associated metamorphic events have been reported in a number of studies in Proterozoic and modern settings (Ham and Bell 2004; Sayab 2005; Aerden and Sayab 2008; Shah et al. 2012; Lahtinen et al. 2014; Deng et al. 2016).

In this study, we addressed the long-standing question concerning the relative timing of dextral versus sinistral movements along the KiSZ. We conclude that the early D1 thrusting phase (ca. 1.92–1.91 Ga) and associated bend in the thrust splay provided the first-order structural control on the localization of

the Suurikuusikko deposit and that fluid flow associated with this early deformation phase deposited refractory gold at the Suurikuusikko deposit and also at the Iso-Kuotko deposit. However, the main gold mineralization event at the Iso-Kuotko deposit occurred during E-W contraction (D5) at ca. 1.77–1.76 Ga that produced widespread veining and associated gold mineralization. Finally, we conclude that the deposition and multiple remobilization processes of ore-bearing fluids are controlled by a succession of near-orthogonal tectonic shortenings, as experienced by the long-lived KiSZ.

References

Aerden DGAM (1993) Formation of massive sulfide lenses by replacement of folds: the Hercules Pb-Zn mine, Tasmania. Econ Geol 88: 377–396. https://doi.org/10.2113/gsecongeo.88.2.377

Aerden D, Sayab M (2008) From Adria- to Africa-driven orogenesis: evidence from porphyroblasts in the Betic Cordillera, Spain. J Struct Geol 30:1272–1287

Aerden DGAM, Sayab M (2017) Probing the prodigious strain fringes from Lourdes. J Struct Geol 105:88–106. https://doi.org/10.1016/j.jsg.2017.11.001

Bartlett WL, Friedman M, Logan J (1981) Experimental folding and faulting of rocks under confining pressure. Part IX. Wrench faults in limestone layers. Tectonophysics 79:255–277

Bell TH (1986) Foliation development and refraction in metamorphic rocks: reactivation of earlier foliations and decrenulation due to shifting patterns of deformation partitioning. J Metamorph Geol 4: 421–444. https://doi.org/10.1111/j.1525-1314.1986.tb00362.x

Bell TH (2010) Deformation partitioning, foliation successions and their significance for orogenesis: hiding lengthy deformation histories in mylonites. Geol Soc Lond Spec Publ 335:275–292. https://doi.org/10.1144/sp335.13

Bell TH, Johnson SE (1992) Shear sense: a new approach that resolves conflicts between criteria in metamorphic rocks. J Metamorph Geol 10:99–124. https://doi.org/10.1111/j.1525-1314.1992.tb00074.x

Bell TH, Rubenach MJ (1983) Sequential porphyroblast growth and crenulation cleavage development during progressive deformation. Tectonophysics 92:171–194. https://doi.org/10.1016/0040-1951(83)90089-6

Bemis SP, Micklethwaite S, Turner D, James MR, Akciz S, Thiele ST, Bangash HA (2014) Ground-based and UAV-based photogrammetry: a multi-scale, high-resolution mapping tool for structural geology and paleoseismology. J Struct Geol 69:163–178. https://doi.org/10.1016/j.jsg.2014.10.007

Billings MP (1954) Structural geology, **2nd edition**. Prentice-Hall, New Jersey

Blenkinsop TG, Doyle MG (2014) Structural controls on gold mineralization on the margin of the Yilgarn craton, Albany-Fraser orogen: the Tropicana deposit, Western Australia. J Struct Geol 67:189–204. https://doi.org/10.1016/j.jsg.2014.01.013

Blenkinsop T, Tripp G, Gillen D (2017) The relationship between mineralization and tectonics at the Kainantu gold–copper deposit, Papua New Guinea. Geol Soc Lond Spec Publ 453:269–288. https://doi.org/10.1144/SP453.11

Blewett RS, Czarnota K, Henson PA (2010) Structural-event framework for the eastern Yilgarn Craton, Western Australia, and its implications for orogenic gold. Precambrian Res 183:203–229. https://doi.org/10.1016/j.precamres.2010.04.004

Burg JP, Wilson CJL (1988) A kinematic analysis of the southernmost part of the Bega Batholith. Aust J Earth Sci 35:1–13. https://doi.org/10.1080/08120098808729435

Deng H, Koyi HA, Nilfouroushan F (2016) Superimposed folding and thrusting by two phases of mutually orthogonal or oblique shortening in analogue models. J Struct Geol 83:28–45. https://doi.org/10.1016/j.jsg.2015.08.005

Eilu P (2007) FINGOLD: brief descriptions of all drilling-indicated gold occurrences in Finland – the 2007 data. Geological Survey of Finland, Report of Investigation 166, Espoo

Gaál G, Berthelsen A, Gorbatschev R, Kesola R, Lehtonen MI, Marker M, Raase P (1989) Structure and composition of the Precambrian crust along the POLAR Profile in the northern Baltic Shield. Tectonophysics 162:1–25. https://doi.org/10.1016/0040-1951(89)90354-5

Goldfarb RJ, Baker T, Dubé B et al (2005) Distribution, character, and genesis of gold deposits in metamorphic terranes. Econ Geol One Hundredth Anniv 1905–2005(100):407–450. https://doi.org/10.5382/AV100.14

Groves DI, Santosh M (2016) The giant Jiaodong gold province: the key to a unified model for orogenic gold deposits? Geosci Front 7:409–417. https://doi.org/10.1016/j.gsf.2015.08.002

Groves DI, Goldfarb RJ, Gebre-Mariam M, Hagemann SG, Robert F (1998) Orogenic gold deposits: a proposed calssification in the context of their crustal contribution and relationship to other gold deposit types. Ore Geol Rev 13:7–27. https://doi.org/10.1016/S0169-1368(97)00012-7

Groves DI, Santosh M, Goldfarb RJ, Zhang L (2018) Structural geometry of orogenic gold deposits: implications for exploration of world-class and giant deposits. Geosci Front 9:1163–1177. https://doi.org/10.1016/j.gsf.2018.01.006

Ham AP, Bell TH (2004) Recycling of foliations during folding. J Struct Geol 26:1989–2009. https://doi.org/10.1016/j.jsg.2004.04.003

Hanski E, Huhma H (2005) Central Lapland greenstone belt. In: Lehtinen M, Nurmi PA, Rämö OT (eds) Precambrian geology of Finland key to the evolution of the Fennoscandian shield. Elsevier, Amsterdam, pp 139–193

Härkönen I, Pankka H, Rossi S (2000) Summary report. The Iso-Kuotko gold prospects, northern Finland. Geological Survey of Finland, Archive Code C/M06/2744/00/1/10, pp 1–18

Hölttä P, Väisänen M, Väänänen J, Manninen T (2007) Paleoproterozoic metamorphism and deformation in Central Lapland, Finland. In: Ojala J (ed) Gold in the Central Lapland Greenstone Belt. Geological Survey of Finland, Special Paper 44, Espoo, pp 7–56

Johnston ST, Weil AB, Gutiérrez-Alonso G (2013) Oroclines: thick and thin. Bull Geol Soc Am 125:643–663. https://doi.org/10.1130/B30765.1

Kojonen K, Johanson B (1999) Determination of refractory gold distribution by microanalysis, diagnostic leaching and image analysis. Mineral Petrol 67:1–19. https://doi.org/10.1007/BF01165112

Koppström K (2012) Electron microprobe and LA-ICP-MS study on the distribution of gold and other elements in pyrite and arsenopyrite from the Suurikuusikko gold deposit, northern Finland. University of Oulu

Kukkonen, I., Lahti, I., Heikkinen, P., Heinonen, S., Laitinen, J. and HIRE working group. 2009. HIRE seismic reflection survey in the suurikuusikko gold mining and exploration area, North Finland. Geophysical Research Report Q23/2009/28: 1-51

Kyle JR, Ketcham RA (2015) Application of high resolution X-ray computed tomography to mineral deposit origin, evaluation, and processing. Ore Geol Rev 65:821–839. https://doi.org/10.1016/j.oregeorev.2014.09.034

Lahtinen R, Johnston ST, Nironen M (2014) The Bothnian coupled oroclines of the Svecofennian Orogen: a Palaeoproterozoic terrane wreck. Terra Nova 26:330–335. https://doi.org/10.1111/ter.12107

Lahtinen R, Sayab M, Karell F (2015) Near-orthogonal deformation successions in the poly-deformed Paleoproterozoic Martimo belt: implications for the tectonic evolution of Northern Fennoscandia. Precambrian Res 270:22–38. https://doi.org/10.1016/j.precamres.2015.09.003

Lahtinen R, Huhma H, Sayab M, Lauri LS, Hölttä P (2018) Age and structural constraints on the tectonic evolution of the Paleoproterozoic Central Lapland Granitoid Complex in the Fennoscandian Shield. Tectonophysics 745:305–325. https://doi.org/10.1016/j.tecto.2018.08.016

Lehtonen M, Airo M-L, Eilu P, et al (1998) The stratigraphy, petrology and geochemistry of the Kittila greenstone area, northern Finland. A report of the Lapland volcanite project. Geological Survey of Finland, Report of Investigation 140, Espoo, p 1–144

Lin S, Williams PF (1992) The origin of ridge-in-groove slickenside striae and associated steps in an S-C mylonite. J Struct Geol 14:315–321. https://doi.org/10.1016/0191-8141(92)90089-F

Luosto U, Flueh ER, Lund CE, Group W (1989) The crustal structure along the POLAR profile from seismic refraction investigations. Tectonophysics 162:51–85. https://doi.org/10.1016/0040-1951(89)90356-9

Luukas J, Kousa J, Nironen M, Vuollo J (2017) Major stratigraphic units in the bedrock of Finland, and an approach to tectonostratigraphic division. In: Nironen M (ed) Bedrock of Finland at the scale 1:1 000 000 - major stratigraphic units, metamorphism and tectonic evolution. Geol Surv Finland Spec Pap 60, Espoo, pp 9–40

Means WD (1987) A newly recognized type of slickenside striation. J Struct Geol 9:585–590. https://doi.org/10.1016/0191-8141(87)90143-X

Molnár F, Middleton A, Stein H, O`Brien H, Lahaye Y, Huhma H, Pakkanen L, Johanson B (2018) Repeated syn- and post-orogenic gold mineralization events between 1.92 and 1.76 Ga along the Kiistala Shear Zone in the Central Lapland Greenstone Belt, northern Finland. Ore Geol Rev 101:936–959. https://doi.org/10.1016/j.oregeorev.2018.08.015

Niiranen T (2015) A 3D structural model of the central and eastern part of the Kittilä terrane. Geological survey of Finland. Archive report 90/2015, Northern Finland Office, pp 1–17

Nironen M (2017) Structural interpretation of the Peräpohja and Kuusamo belts and Central Lapland, and a tectonic model for northern Finland. Geological Survey of Finland, Report of Investigation 234, Espoo, pp 1–53

Patison NL (2007) Structural controls on gold mineralisation in the Central Lapland Greenstone Belt. In: Ojala J (ed) Gold in the Central Lapland Greenstone Belt. Geological Survey of Finland, Special Paper 44, Espoo, pp 107–122

Patison NL, Salamis G, Kortelainen VJ (2007) The Suurikuusikko gold deposit: project development summary of northern Europe's largest gold deposit. In: Ojala J (ed) Gold in the Central Lapland Greenstone Belt. Geological Survey of Finland, Special Paper 44, Espoo, pp 125–134

Rastas P, Huhma H, Hanski E, et al (2001) U-Pb isotopic studies on the Kittilä greenstone area, central Lapland, Finland. In: Vaasjoki M (ed) Radiometric age determinations from Finnish Lapland and their bearing on the timing of Precambrian volcano-sedimentary sequences. Geol Surv Finland Spec Pap 33, pp 95–141

Rosenbaum G (2014) Geodynamics of oroclinal bending: insights from the Mediterranean. J Geodyn 82:5–15. https://doi.org/10.1016/j.jog.2014.05.002

Sayab M (2005) Microstructural evidence for N-S shortening in the Mount Isa Inlier (NW Queensland, Australia): the preservation of early W-E-trending foliations in porphyroblasts revealed by independent 3D measurement techniques. J Struct Geol 27:1445–1468. https://doi.org/10.1016/j.jsg.2005.01.013

Sayab M (2008) Correlating multiple deformation events across the Mesoproterozoic NE Australia using foliation intersection axes (FIA) preserved within porphyroblasts. Gondwana Res 13:331–351

Sayab M, Suuronen J, Hölttä P et al (2015) High-resolution X-ray computed microtomography : a holistic approach to metamorphic fabric analyses. Geology 43:55–58. https://doi.org/10.1130/G36250.1

Sayab M, Suuronen JP, Molnár F, Villanova J, Kallonen A, O'Brien H, Lahtinen R, Lehtonen M (2016) Three-dimensional textural and quantitative analyses of orogenic gold at the nanoscale. Geology 44:739–742. https://doi.org/10.1130/G38074.1

Sayab M, Miettinen A, Aerden D, Karell F (2017) Orthogonal switching of AMS axes during type-2 fold interference: insights from integrated X-ray computed tomography, AMS and 3D petrography. J Struct Geol 103:1–16. https://doi.org/10.1016/j.jsg.2017.09.002

Sayab M, Aerden D, Paananen M, Saarela P (2018) Virtual structural analysis of Jokisivu open pit using "structure-from-motion" unmanned aerial vehicles (UAV) photogrammetry: implications for structurally-controlled gold deposits in Southwest Finland. Remote Sens 10:1–17. https://doi.org/10.3390/rs10081296

Shah SZ, Sayab M, Aerden D, Iqbal Q (2012) Formation mechanism and tectonic significance of millipede microstructures in the NW Himalaya. J Asian Earth Sci 59:3–13. https://doi.org/10.1016/j.jseaes.2012.05.001

Snavely N, Seitz SM, Szeliski R (2008) Modeling the world from internet photo collections. Int J Comput Vis 80:189–210. https://doi.org/10.1007/s11263-007-0107-3

Suuronen J-P, Sayab M (2018) 3D nanopetrography and chemical imaging of datable zircons by synchrotron multimodal X-ray tomography. Sci Rep 8:4747. https://doi.org/10.1038/s41598-018-22891-9

Tomkins AG (2013) On the source of orogenic gold. Geology 41:1255–1256. https://doi.org/10.1130/focus122013.1

Väisänen M (2002) Structural features in the Central Lapland Greenstone Belt, Northern Finland. Geological Survey of Finland, K21.42/2002/3, Espoo, pp 1–20

Vielreicher NM, Groves DI, McNaughton NJ (2016) The giant Kalgoorlie gold field revisited. Geosci Front 7:359–374. https://doi.org/10.1016/j.gsf.2015.07.006

Ward P, Härkönen I, Nurmi PA, Pankka HS (1989) Structural studies in the Lapland greenstone belt, northern Finland and their application to gold mineralization. In: Autio S (ed) Current research. Geological Survey of Finland, Special Paper 10, Espoo, pp 71–77

Westoby MJ, Brasington J, Glasser NF, Hambrey MJ, Reynolds JM (2012) "Structure-from-motion" photogrammetry: a low-cost, effective tool for geoscience applications. Geomorphology 179:300–314. https://doi.org/10.1016/j.geomorph.2012.08.021

Wyche NL, Eilu P, Koppström K, Kortelainen VJ, Niiranen T, Välimaa J (2015) The Suurikuusikko gold deposit (Kittilä Mine), Northern Finland. In: Maier W, Lahtinen R, O'Brien H (eds) Mineral deposits of Finland. Elsevier Inc., Amsterdam, pp 411–433

Yardley BWD, Cleverley JS (2015) The role of metamorphic fluids in the formation of ore deposits. Geol Soc Lond Spec Publ 393:117–134. https://doi.org/10.1144/SP393.5

Springer